THE PROCEEDINGS OF
THE PHYSICAL SOCIETY
Section B

VOL. 62, PART 6 1 June 1949 No. 354 B

The Production of Sprays and Mists of Uniform Drop Size by Means of Spinning Disc Type Sprayers

BY W. H. WALTON* AND W. C. PREWETT
Chemical Defence Experimental Station, Porton, Wilts.

MS. received 13*th September* 1948, *in amended form* 16*th November* 1948.

ABSTRACT. Spray of almost uniform drop size is formed when liquid is fed under suitable conditions on to the centre of a rotating disc and centrifuged off the edge. This method of spraying has been studied over a wide range of variables and homogeneous clouds have been produced in the drop-size range from 3 mm. to 15 μ diameter. The size of the spray drops is given approximately by the equation $d=3{\cdot}8\ (\mathrm{T}/\mathrm{D}\rho)^{\frac{1}{2}}/\omega$ where d=drop diameter, D=disc diameter, ω=angular velocity of disc, T=surface tension of liquid, ρ=density of liquid. The spray thus formed also contains a proportion of fine satellite drops, but their smaller distance of projection from the disc enables them to be removed from the cloud when their presence is undesirable. Relatively coarse sprays are easily produced by means of a simple electric motor-driven disc. The finer spray sizes require rotor speeds up to several thousands of revolutions per second and high speed air driven " tops " have been used for this purpose. Suitable designs of apparatus are described.

---

§ 1. INTRODUCTION

IN the course of certain experiments requiring the controlled dispersion of liquid insecticides (Johnson and Walton 1947) it was noted that spray of almost uniform drop size could be produced by means of a spinning disc sprayer of the well known type in which liquid is fed on to the centre of a rotating disc and centrifuged off the edge in droplet form. It was found, moreover, that the drop size was independent of the flow rate over a wide range and could be readily varied by altering the speed of rotation of the disc. This was in striking contrast to other methods of liquid disruption, which invariably give widely heterogeneous dispersions. The phenomenon has, therefore, been studied in greater detail with a view to developing apparatus for the production of homogeneous droplet clouds over as wide a size range as possible. It was felt that such spray sources would be of value in many fields of research. The drop size range so far covered is from several millimetres diameter down to about 15 μ. Smaller solid or liquid particles can be produced by spraying solutions and using the evaporation of solvent to give a further reduction in particle size. For the finer drops very high revolutionary speeds are required, and recourse has been made to air-driven tops capable of giving speeds up to several thousands of revolutions per second and radial accelerations of the order of a million times gravity. For lower speeds and larger drops, an ordinary electric motor drive is adequate.

[*] Now with Scientific Department, National Coal Board.

Rotating disc sprayers have been well known for many years and are in widespread industrial use for such purposes as air humidification and spray-drying, but their ability to deliver homogeneous spray does not seem to have been generally realized. For example, Houghton (1941), in a review article discussing various spraying means, states that the drop size distribution of a rotating nozzle (spinning disc) is quite similar to that of a pressure nozzle. This probably applies to high high rates of liquid flow. Homogeneous spray is only obtained at comparatively low flow rates.

§2. BASIC DESIGN OF APPARATUS

The rotors used for delivering homogeneous spray may have a variety of surface profiles and types of edge, but the spraying performance does not depend to any marked degree on these characteristics as shown in §§3 and 4. For purposes of standardization, however, rotors with plane, smooth-turned surfaces have been used, the periphery of the larger motor-driven ones being turned to a sharp 45° edge and the air-driven tops to a sharp 90° edge, as illustrated in Figure 1.

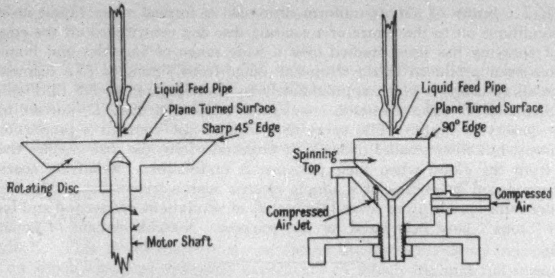

Spinning disc sprayer. Vertical section (diagrammatic). Spinning top sprayer. Vertical section (diagrammatic).

Figure 1.

The liquid is fed from a small-bore metal tube on to the centre of the rotating surface and spreads over it to the periphery in a thin film. Care should be taken to see that the feed is central and continuous and that the rotor surface is completely wetted by the liquid, otherwise an uneven film and non-uniform dispersion may result.

§3. SPRAYING CHARACTERISTICS

(i) *Satellite Drops and their Removal*

The spray projected from the rotor always contains a number of fine satellite drops in addition to the main homogeneous cloud, but the percentage of sprayed liquid in the satellites is very small provided that the rate of liquid flow is not too high. Owing to their small mass, the satellites are projected a much smaller distance from the rotor than are the main drops and this enables them to be separated from the cloud if their presence is undesirable. This is illustrated in Figure 2 (Plate), which shows sectors of the circular patterns produced by the spray from a disc revolving at various speeds falling on a horizontal sheet of absorbent paper. The disc was situated 1 m. vertically above the left-hand end of the paper strip in each case. The main drops and satellites are seen lying in two well-separated bands, and the narrowness of the band containing the main drops gives a good indication of their homogeneity of size. In this example the diameter of the main drops diminishes from 1·56 mm. to 0·36 mm. as the speed of the disc is increased from 600 r.p.m. to 2,500 r.p.m., but their distance of projection passes through a maximum at 1,500 r.p.m. Separation of the main and satellite drops can be achieved quite simply by placing under the apparatus a horizontal sheet of card or metal having an aperture cut at an appropriate point so that the main drops fall through it whereas the satellites are intercepted. At very high revolutionary speeds such as are produced by the air driven spinning top sprayer, the drop size is very small and the particles are substantially airborne so that the above procedure for removing the satellites cannot be adopted. Separation can be effected by surrounding the apparatus with a cylindrical sleeve having an annular gap, the sleeve being of such a diameter that the main drops are projected through the gap but the satellites come to rest within the sleeve. An indrawn current of air through the gap then removes the unwanted satellites from the cloud. An apparatus incorporating this principle is described in §5 (ii). The radial distances of projection of water and methyl salicylate drops from discs of various diameters at speeds up to 4,000 r.p.m. are shown in Figures 3 and 4 respectively. These were measured on a sheet of paper placed 1 m. below the disc. Figure 5 gives data for the distance of projection of dibutyl phthalate drops from a spinning top of 3 cm. diameter running at speeds up to 1,500 r.p.s. (90,000 r.p.m.).

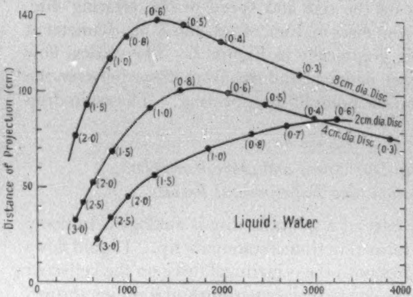

Figure 3.

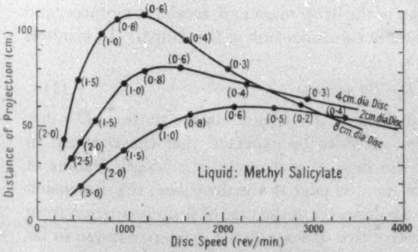

Figures 3 and 4. Spinning disc sprayer. Distance of projections of drops from spinning disc. Figures in brackets denote the corresponding drop size in mm. diameter.

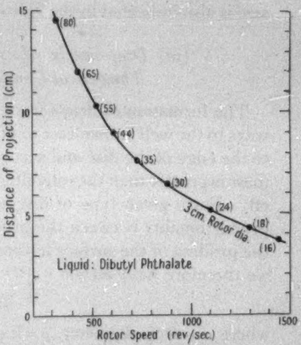

Figure 5. Spinning top sprayer. Distance of projection of drops from high speed rotor. Figures in brackets denote the corresponding drop size in microns diameter.

(ii) *Influence of Rate of Liquid Feed*

The effect of the rate of liquid feed on the composition of the spray at a constant disc speed is shown in Figure 6 (Plate), which was obtained in a similar manner to that employed for Figure 2. In this figure the stains from the main drops have coalesced to form a continuous band. It will be noted that the distance of projection and therefore the size of the main drops remains unchanged but that the satellites increase in size, size-range, and quantity as the flow rate is increased. At high flow rates a continuous spectrum of drop-sizes is produced and separation of the satellites from the main drops becomes impossible. The maximum flow rate at which satisfactory separation of the main homogeneous drops from the satellites can be achieved depends on the size and speed of the rotating disc. Data for methyl salicylate sprayed from discs of 2 cm., 4 cm. and 8 cm. diameter at speeds up to 4,000 r.p.m. are shown graphically in Figure 7. The critical flow rate was taken as that at which the well defined band free from drops between the satellites and the main cloud was on the point of disappearing. The main drop size is also indicated in the figure.

(iii) *Drop-size in relation to Disc Speed and other Variables. Theoretical Considerations and Experimental Results*

The formation of drops from the edge of a spinning disc is analogous in many ways to the well known case of drop formation from a stationary tip. Liquid flows to the edge of the disc and accumulates until the centrifugal force on the collected mass is greater than the retaining forces due to surface tension and it is then thrown off. For a given type of disc edge profile it is therefore reasonable to expect a proportionality between the product of the drop mass and accelerating force, and the product of the surface tension and linear dimension of the drops. In symbols we therefore have $\pi d^3\rho/6 \times \omega^2 D/2 \propto Td$,

$$d\omega(D\rho/T)^{\frac{1}{2}} = \text{const.}, \qquad \ldots\ldots(1)$$

where d = drop diameter, ρ = liquid density, T = liquid surface tension, D = disc diameter, ω = disc angular velocity. It is to be expected that the constant in equation (1) will be a function of the ratio of a characteristic length (radius of curvature) defining the sharpness of the disc edge to the drop size, the dimension of the edge playing a part similar to tip diameter in the case of drop formation from a tip. Experiment has shown however that at least in the drop-size range so far investigated edge profile is a variable of minor importance.

The validity of equation (1) has been tested experimentally over as wide a range of variables as possible, ω from 50 to 10,000 radians per second, D from 2 cm. to 8 cm., ρ from 0·9 to 13·6 gm/cm^3, T from 31 to 465 dynes/cm., and d from 0·3 to $1{\cdot}2 \times 10^{-3}$ cm. The results are given in Tables 1 and 2. The last columns of the tables give calculated values of $\omega d(D\rho/T)^{\frac{1}{2}}$ which is seen to be nearly constant as required by equation (1). The average value of the constant is about 3·8, and the maximum and minimum values over the whole range investigated are 6·55 and 2·67. $\omega d(D\rho/T)^{\frac{1}{2}}$ appears in general to be rather greater for the high speed air-driven top than for the lower speed motor-driven disc, the average values being 4·5 and 3·3 respectively. The reason for this is not fully understood, but a contributing factor may be the failure of the liquid to pick up the full rotational velocity of the rotor in the former case. In this event one would expect the constant to tend to increase with increasing rotor speed. This effect is noticeable in a

SPINNING DISC SPRAYER

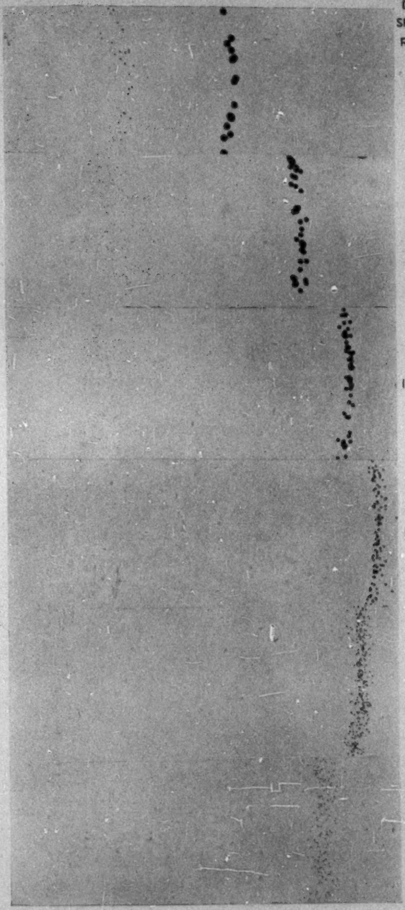

DISC SPEED R.P.M.	DROP DIAM M.M.	DISTANCE OF PROJECTION CM.
600	1·56	51
800	1·17	64
1000	0·95	76
1500	0·61	82
2000	0·42	77
2500	0·36	69

FIG. 2

EFFECT OF DISC SPEED ON DROP SIZE AND DISTANCE OF PROJECTION

(LIQUID, METHYL SALICYLATE; FEED 20 CC/MIN; DISC DIAM 4 CM.)

SPINNING DISC SPRAYER

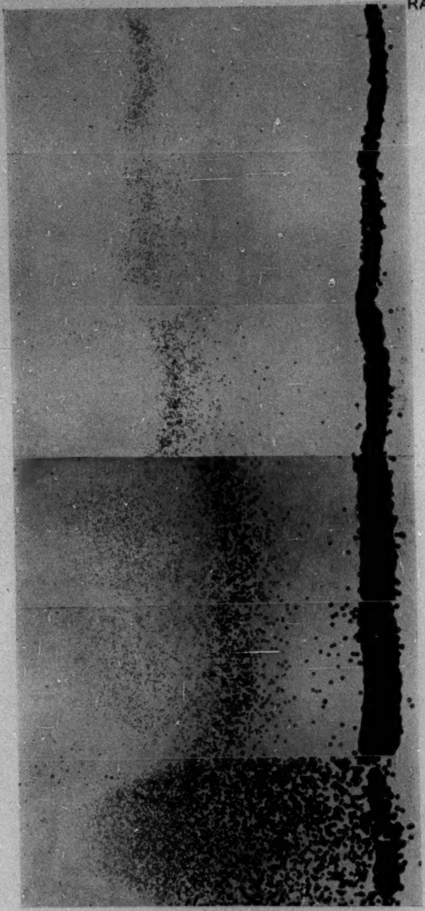
RATE OF LIQUID FEED
0·04 CC/SEC
0·2 CC/SEC
0·4 CC/SEC
1·2 CC/SEC
1·8 CC/SEC
2·8CC/SEC

FIG 6

EFFECT OF RATE OF LIQUID FEED

(LIQUID, METHYL SALICYLATE ; DISC DIAM 4CM, SPEED 1000 R.P.M.)

number of instances in Table 2 but not invariably. The degree of "slip" of the liquid on the rotor surface depends among other things on the rate of flow of the liquid. This was not measured in all the experiments recorded.

It will be noted that viscosity does not appear as a variable in equation (1). Within limits viscosity appears to have little effect on the spraying process as will be seen by reference to Tables 1 and 2, where the viscosities of the liquids used are recorded. The range of values covered is from 0·01 to 15 poise. A high viscosity, however, does tend to increase the proportion of satellites in the spray and to reduce the maximum flow rate at which homogeneous drops are formed, but the effect is complex and has not been analysed in our experiments.

Table 1. Spinning Disc Sprayer.

Methyl salicylate (dyed). $T=39{\cdot}2$ dyne/cm. $\rho=1{\cdot}18$ gm/cm^3. $\eta=0{\cdot}033$ poise.

(1)	(2)	(3)	(4)	(1)	(2)	(3)	(4)	(1)	(2)	(3)	(4)
2	500	2800	3·58	4	400	2300	3·34	8	300	2000	3·07
2	750	1830	3·51	4	600	1560	3·39	8	400	1610	3·30
2	1000	1380	3·53	4	800	1200	3·48	8	600	1190	3·67
2	1500	900	3·47	4	1000	950	3·44	8	800	870	3·57
2	2000	640	3·39	4	1500	610	3·32	8	1000	710	3·63
2	2500	510	3·27	4	2000	480	3·49	8	1500	420	3·23
2	3000	470	3·61	4	2500	340	3·08	8	2000	310	3·13
2	3500	400	3·58	4	3000	290	3·16	8	2500	240	3·07
2	4000	320	3·29					8	3000	190	3·91

Mercury $T=465$ dyne/cm. $\rho=13{\cdot}55$ gm/cm^3. $\eta=0{\cdot}016$ poise.

8	660	1020	3·40	8	1584	400	3·20	8	2280	270	3·11
8	1050	570	3·19	8	1840	350	3·25	8	2850	210	3·03
8	1290	480	3·12								

Water. $T=73$ dyne/cm. $\rho=1$ gm/cm^3. $\eta=0{\cdot}01$ poise.

2	650	3000	3·36	4	450	2840	3·13	8	400	2100	2·90
2	800	2410	3·33	4	600	2100	3·09	8	600	1320	2·73
2	1000	1880	3·25	4	800	1600	3·17	8	800	1000	2·76
2	1500	1280	3·33	4	1000	1200	2·93	8	1000	770	2·67
2	2000	920	3·18	4	1500	840	3·08	8	1500	520	2·70
2	3000	640	3·32	4	2000	620	3·04	8	2000	400	2·77
				4	3000	400	2·93	8	3000	280	2·90
				4	4000	280	2·74				

Dibutyl phthalate + 1% waxoline blue. $T=34{\cdot}0$ dyne/cm. $\rho=1{\cdot}046$ gm/cm^3.
$\eta=0{\cdot}26$ poise.

5	1500	600	3·70	5	3000	290	3·58	5	4500	200	3·70
5	2000	430	3·54	5	3500	250	3·60	5	5000	190	3·91
5	2500	360	3·70	5	4000	220	3·62	5	6000	180	4·44

(1) Disc dia. (cm.) (2) Disc speed (rev/min.) (3) Drop dia. (μ) (4) $\omega d\,(D\rho/T)^{\frac{1}{2}}$

The data for dibutyl phthalate were kindly provided by Mr. M. Ainsworth.

§4. MECHANISM OF DROP FORMATION

The mechanism of drop formation from an edge and the effect of edge profile have been examined in greater detail by allowing a film of water to flow under gravity over a vertical metal sheet and to drip from the lower edge. This process is similar to that of drop formation from a spinning disc except that gravity is substituted for the centrifugal acceleration $\omega^2 D/2$. The lower edge of the sheet, which was horizontal, was bent to various shapes, and the resulting drop size was found by catching and weighing ten drops. The results are given in Table 3.

Table 2. Spinning Top Sprayer (rotor dia. 3 cm.)

(1)	(2)	(3)	(1)	(2)	(3)	(1)	(2)	(3)
Methyl salicylate/paraffin (25/75). $T=34{\cdot}9$ dyne/cm. $\rho=0{\cdot}929$ gm/cm^3. $\eta=0{\cdot}118$ poise.								
303	85	4·49	1030	20	3·66	1391	16	3·96
556	45	4·44	1120	20	3·98	1500	13·5	3·60
760	30	4·06	1261	16	3·60	1641	12·2	3·56
916	22	3·59						
Glycerine. $T=63{\cdot}4$ dyne/cm. $\rho=1{\cdot}26$ gm/cm^3. $\eta=15$ poise.								
340	90	4·68	900	35	4·83	1500	25	5·75
6000	55	5·05						
o–dichlor–benzene. $T=34{\cdot}2$ dyne/cm. $\rho=1{\cdot}30$ gm/cm^3.								
340	52	3·75	900	27	5·15	1500	20	6·36
600	37	4·71						
Ethylene dibromide. $T=38{\cdot}8$ dyne/cm. $\rho=2{\cdot}13$ gm/cm^3. $\eta=0{\cdot}016$ poise.								
340	37	3·03	900	20	4·60	1500	17	6·55
600	27	4·13						
Dekalin. $T=31{\cdot}5$ dyne/cm. $\rho=0{\cdot}896$ gm/cm^3. $\eta=0{\cdot}017$ poise.								
340	65	4·06	900	30	4·95	1500	20	5·50
600	45	4·95						
Dibutyl phthalate. $T=34{\cdot}0$ dyne/cm. $\eta=1{\cdot}046$ gm/cm^3. $\eta=0{\cdot}264$ poise.								
328	80	5·16	610	44	5·10	1100	24	5·04
440	65	5·46	730	35	4·87	1290	18	4·44
530	55	5·56	880	30	5·04	1440	16	4·40
Tricresyl phosphate. $T=43{\cdot}2$ dyne/cm. $\rho=1{\cdot}188$ gm/cm^3. $\eta=1{\cdot}42$ poise.								
340	90	5·52	900	25	4·07	1500	20	5·42
600	37	4·01						
Methyl salicylate. $T=39{\cdot}2$ dyne/cm. $\rho=1{\cdot}18$ gm/cm^3. $\eta=0{\cdot}0376$ poise.								
340	60	3·85	900	30	5·10	1500	18	5·08
600	42	4·74						
Mercury. $T=465$ dyne/cm. $\rho=13{\cdot}55$ gm/cm^3. $\eta=0{\cdot}016$ poise.								
520	32	3·19	850	21	3·36	1020	16	3·05

(1) Disc speed (rev/sec.) (2) Drop dia. (μ) (3) $\omega d\,(D\rho/T)^{\frac{1}{2}}$

While the drop size varies to some extent with the nature and characteristic dimension of the edge the dependence is very much less than in the case of tips. The maximum deviation, for the right angle edge, from the mean drop diameter is only 8%. Experiments have been carried out with spinning tops having edges of various profiles but no difference in drop size was noted. Drop size was estimated by impaction of the drops on magnesium oxide coated slides and measurement of the crater diameter as described by May (1945). Variations of the order of 8% would probably have escaped detection.

It is of interest to compare the size of the above mentioned water drops from a stationary sheet with that produced by a rotating disc. If g is substituted for $\omega^2 D/2$ in equation (1), the expression on the left-hand side becomes $d(2g\rho/T)^{\frac{1}{2}}$. Substitution of $d=0{\cdot}726$ as given in Table 3, $g=981$, $\rho=1$, $T=73$ gives the numerical value 3·76, which accords well with the values of $\omega d(D\rho/T)^{\frac{1}{2}}$ for the spinning disc and top given in Tables 1 and 2. In the case of the stationary metal sheet the process of drop formation can be followed visually. The liquid film flows to the lower edge of the sheet and collects there as a pendent cylinder. This cylinder of liquid grows until a critical size is reached when it collapses and a drop is released. As a very simple physical picture, the cylinder may be imagined to grow until the weight per unit length is just equal to the surface tension force acting vertically on either side, i.e. the cylinder will break away from the edge when

Table 3. Formation of Drops at Lower Edge of Vertical Metal Sheet

Edge profile		Drop weight (gm.)	Drop diameter (cm.)
Sharp	|	0·176	0·695
Right angle	_|	0·253	0·785
45°	√	0·169	0·686
Round, 6 cm. radius	J	0·225	0·755
Round, 0·5 cm. radius	J	0·187	0·709
		Mean 0·202	Mean 0·726

$$\pi a^2 \rho g = 2T \qquad \ldots\ldots(2)$$

where a is the mean radius of the cylinder. As is well known a long cylinder of liquid is unstable under surface tension force and breaks up to form discrete drops.

The "wavelength" of the break-up depends to some extent on the nature of the initial disturbances. The shortest unstable sections into which the cylinder can break have a length of $2\pi a$, but Rayleigh (1879) has shown that the length of disturbance of maximum rate of growth is $9{\cdot}0a$. The former value would lead to a drop size (diameter) given by $\pi d^3/6=2\pi a\,.\,\pi a^2$, or $d=(12\pi)^{\frac{1}{3}}a$ whence from equation (2) $d(2g\rho/T)^{\frac{1}{2}}=(4/\pi)^{\frac{1}{2}}(12\pi)^{\frac{1}{3}}=3{\cdot}79$. This is in very close agreement with the mean experimental value 3·76 given above. The corresponding theoretical value for a break-up length of $9{\cdot}0\,a$ is 4·26.

Identical reasoning applied to the spinning disc leads to the substitution of $\omega^2 D/2$ for g, giving $\omega d(D\rho/T)^{\frac{1}{2}}=3{\cdot}79$ for a break-up length of $2\pi a$, and 4·26 for a break-up length of $9{\cdot}0a$. Both these values lie within the experimentally determined range for the spinning disc. It seems, therefore, that this simple physical picture can be taken as a substantially accurate representation of the mechanism of drop formation.

Merrington and Richardson (1947) have recently investigated the break-up of liquid jets in air. They found that whereas high speed jets are disrupted into heterogeneous spray depending on the velocity of the jet relative to the air, below a limiting velocity the drops from narrow jets become uniform in size. For a number of liquids and nozzle diameters the ratio of this uniform drop diameter to the jet diameter was approximately constant, the average value being 2·1. This corresponds to a break up of the jet into lengths of approximately 12*a*, which is rather greater than Rayleigh's theoretical value.

It is believed that spray of uniform size is produced by the spinning disc only when drops are formed and released individually from the disc edge, the rate of flow of liquid to the edge being small so that centrifugal and surface tension forces acting on the growing drops are substantially in equilibrium up to the time of break-away. At higher rates of flow inertia forces become important and the fluid leaves the disc edge as a thin sheet which breaks up into spray with the usual broad drop-size distribution.

§ 5. CONSTRUCTIONAL DETAILS

(i) *Motor-driven Disc Sprayer*

The design and construction of the motor-driven disc type of sprayer calls for little further comment. Discs of a wide range of diameter can be used, the choice depending on the required output and permissible distance of projection of the drops, for which data are given in Figures 3, 4 and 7. The smallest drop size that can be produced is limited only by the maximum revolutionary speed obtainable.

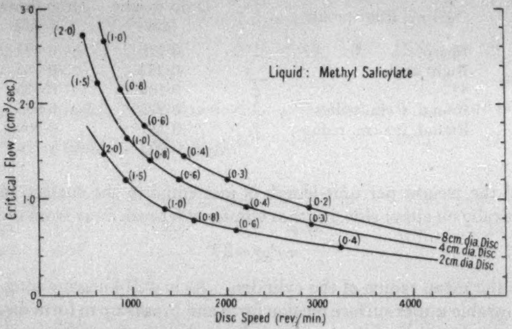

Figure 7. Spinning disc sprayer. Critical flow rate for satisfactory separation of main drops from satellites.

N.B.—Figures in brackets denote the corresponding drop size in mm. diameter.

(ii) *Air-driven Spinning Top Sprayer*

Constructional details for high-speed, self-balancing, air-driven tops have been given by Beams (1937) and others, and these have been followed in constructing the tops used in the present work. A top of this type suitable for use when it is not essential to remove the satellite drops from the spray is shown diagrammatically in Figure 1. The diameter of the rotor is $1\frac{1}{8}$ in. and it is driven by five air jets, from holes 0·029 in. diameter, impinging on the rotor cone half way up its slant surface at an angle of 35° below horizontal in a vertical plane and at 80° to the radius in a horizontal plane. The angles of the rotor and stator cones are 102° and 91° respectively.

The constructional arrangement used for separating satellite drops from the spray is shown in Figure 8. Its basic features are a top similar to that described above, surrounded by a close fitting baffle to deflect escaping compressed air away from the spray. Around this is an outer sleeve forming at its upper end an annular gap through which the main spray drops are projected. An independent source of suction is used to draw away satellite drops which are not projected beyond the sleeve.

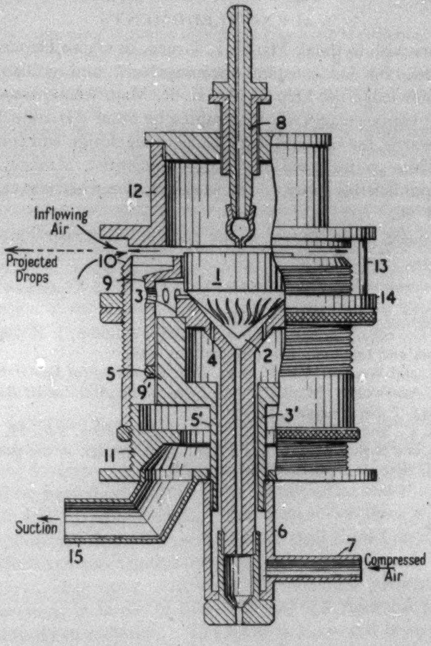

Figure 8. Spinning top sprayer with satellite drop extractor.

It is to be emphasized that the apparatus here described is in an early stage of development and that there is scope for improving both the performance and the mechanical construction. Recent work by Mr. K. R. May on an improved mechanical design indicates that it will be possible to utilize the escaping compressed air to induce the satellite separating flow without need for an independent source of suction.

§ 6. APPLICATIONS

Homogeneous spray apparatus of the type described in this paper has already found application in a number of fields of research. In its original application to which reference has already been made, Johnson and Walton (1947) used a motor-driven disc sprayer in an investigation of the most effective drop size, area dosage, and solution concentration for sprayed D.D.T. solutions used to kill mosquito larvae under natural conditions. Parr and Busvine (1949) have used the method to prepare standardized deposits of insecticides on various surfaces for entomological tests, and Kennedy, Ainsworth and Toms (1948) have employed it for the experimental spraying of locusts. The air-driven top has been used by Prewett and Walton (unpublished work) to produce homogeneous clouds of solid particles for the testing of cloud sampling apparatus. Other applications include its use in researches on disinfectant mists and similar problems.

ACKNOWLEDGMENTS

The authors wish to thank Mr. H. L. Green, in whose Department this work was carried out, for his constant encouragement and guidance. They also gratefully acknowledge the help of Mr. K. R. May, whose association with the experiments at various stages was interrupted by other war-time demands, and of Mr. H. V. Edwards, for valuable suggestions in the design and construction of the apparatus. They are indebted to the Chief Scientist, Ministry of Supply, for permission to publish this paper. The work here described was carried out during the years 1944–46.

The "spinning top" sprayer is the subject of British Patent Application, No. 7112/47.

REFERENCES

Beams, J. W., 1937, *J. Appl. Phys.*, **8**, 795.
Houghton, H. G., 1941, *Chemical Engineers Handbook* (Editor, J. H .Perry), 2nd Edition (New York and London : McGraw Hill), p. 1984.
Johnson, C. G., and Walton, W. H., 1947, *Bull. Entomological Research*, **38**, 405.
Kennedy, J. S., Ainsworth, M., and Toms, B. A., 1948, *Anti-Locust Bull.*, **2.**
May, K. R., 1945, *J. Sci. Instrum.*, **22,** 187.
Merrington, A. C., and Richardson, E. G., 1947, *Proc. Phys. Soc.*, **59,** 1.
Parr, H. C. M., and Busvine, J. R., 1949, *Ann. Appl. Biology*, in the press.
Rayleigh, Lord, 1879, *Proc. Lond. Math. Soc.*, **10,** 4.

Dynamic Impedance and Sensitivity of Radiation Thermocouples

By P. B. FELLGETT
Peterhouse, Cambridge

Communicated by G. B. B. M. Sutherland; MS. received 15*th October* 1947;
in amended form 8*th October* 1948

ABSTRACT. The concept of dynamic impedance is applied to radiation thermocouples. An equivalent circuit is derived, in terms of which the working of a thermocouple and the factors leading to high sensitivity can be visualized. Methods are given for measuring the dynamic impedance and it is shown that these measurements lead to values for thermo-electric power, heat loss from the receiver, and time constant of the thermocouple. Expressions are given, in terms of the dynamic impedance, for the important properties of radiation thermocouples, namely the signal-to-noise sensitivity, ultimate sensitivity, noise factor and power efficiency. These properties are thus obtained in terms of parameters that can be predicted from the design, or measured in the finished instrument. The sensitivity is found without recourse to micro-measurements and therefore independent of limitations set by the thermocouple amplifier. The expression for sensitivity differs from those previously published, and the discrepancy is discussed. The way in which the ultimate sensitivity might be approached in practice is indicated. The efficiency is shown to depend on the amount of radiation falling on the receiver of the thermocouple, but to be a constant fraction of the thermodynamic limit $\Delta T/T$. For an ideal thermocouple the fraction is one-half, for an actual thermocouple it is less by a factor which we call the relative efficiency.

---

§1. INTRODUCTION

The term "thermocouple" is here used to refer to the high sensitivity type of radiation thermocouple or thermopile as employed, for example, in infra-red spectroscopy. When a thermocouple is carrying a current, its junctions will be heated or cooled by the Peltier effect and this will give rise to thermo-electric E.M.F.'s in the circuit. It is evident that these will be in such a direction as to oppose the flow of current, and we shall show that under practical conditions, the effect is proportional to current. It can consequently be interpreted as due to a dynamic impedance, which the thermocouple presents, in addition to its ohmic resistance, in virtue of those thermal and electrical properties that result in its sensitivity to radiation. The name is borrowed from the analogous case of electro-mechanical transducers.

In this paper the attempt is made by the introduction of the idea of dynamic impedance, to develop the theory of radiation thermocouples in a compact and unified manner. Not all the results presented here are new. In particular, the author believes that the expression for ultimate sensitivity was first published by Milatz and Van der Velden (1943). The present investigation was made in ignorance of their work, and the method is independent.

The present author does not agree with the expressions for thermocouple sensitivity that have hitherto been published. These can be shown to lead to different values for the short- and open-circuit sensitivities contrary to Thévenin's theorem. A new formula is derived, which is actually less complicated, and which makes these sensitivities identical. The reasons for the discrepancy are discussed.

The investigation begins with a discussion of electrothermal analogies.

§2. HEAT CIRCUITS

The flow of heat in a conductor and its storage in a thermal capacity are subject to the same laws as the corresponding electrical phenomena. The analogy can conveniently be set up in two ways. If quantity of heat q is regarded as analogous to quantity of electricity Q, a system results that is most simply related to practical measurements, and which may be called the practical system. More simple theoretical relations result if q/T, which may be thought of as entropy, is related to Q. This may be called the absolute system. In both cases temperature difference ΔT is taken as the analogue of voltage.

Then in the practical system we have

Heat current $W = dq/dt$,
Heat resistance $z = \Delta T/W$,
Thermal capacity $c = q/\Delta T$.

In the absolute system the corresponding quantities are respectively

$$_{a}W = \frac{1}{T}\frac{dq}{dt} = \frac{W}{T}, \qquad _{a}z = \frac{\Delta T}{_{a}W} = Tz, \qquad _{a}c = \frac{q}{\Delta T \, . \, T} = \frac{c}{T}.$$

Using either system, sources of heat are represented as voltage generators, paths of heat flow as heat resistances, and thermal capacities as condensers to ground. There is no thermal analogue of electrical inductance. In this way the thermal behaviour of a thermocouple is represented by the circuit shown in Figure 2.

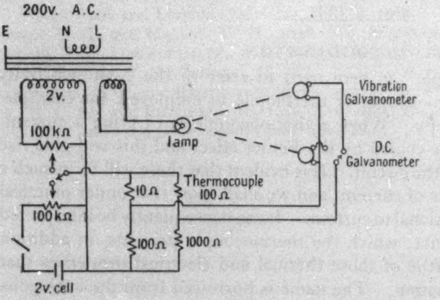

Figure 1. Bridge for measurement of dynamic impedance.

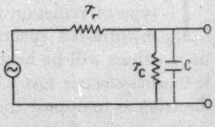

Figure 2. Thermal circuit of thermocouple.

§3. DYNAMIC IMPEDANCE AND ELECTROTHERMAL LOADING OF A THERMOCOUPLE

Consider a thermocouple having a heat resistance z °c./watt between the receiver and its surroundings, total thermo-electric power of the junction S volts/°c. and ohmic resistance R_0 ohms. Then the Peltier coefficient will be TS, and the heating of the junction when the thermocouple carries a current i is

$$W = iST + ki^2R, \qquad \ldots\ldots(3.1)$$

where k is the fraction of the ohmic heat that flows to the junction.

It can be verified that for any practical thermocouple currents of the order of a tenth of a milliampere are sufficiently small that the ohmic heating will be negligible compared with the Peltier effect. Since the currents involved in actual use are some hundreds of times smaller than this, we write

$$W = iST.$$

Temperature rise $$\Delta T = iSTz. \tag{3.2}$$

Thermo-electric E.M.F. generated $$E = iS^2Tz. \tag{3.3}$$

This E.M.F. is evidently in such a direction as to oppose the current flow; and since it is proportional to the current, it may be interpreted as due to a dynamic resistance (additional to the ohmic resistance) given by

$$R_{\mathrm{D}} = E/i = S^2Tz, \tag{3.4}$$

$$= S^2\,{}_{a}z. \tag{3.5}$$

For a thermopile consisting of two or more junctions, the dynamic impedance of the whole is the sum of the R_{D} of the separate junctions, or may be obtained from the overall properties. For example, if there are n identical junctions, the R_{D} of each junction is $(R_{\mathrm{D}})_1 = S^2Tz$. The overall thermo-electric power will be nS and the total heat loss resistance z/n. The total dynamic impedance is therefore

$$(R_{\mathrm{D}})_n = n^2S^2T(z/n) = nS^2Tz = n(R_{\mathrm{D}})_1.$$

We now calculate the effect of the electrical circuit on the thermal behaviour of the receiver. Let radiation fall on the receiver so that the temperature rise ΔT is produced. Then if the external load resistance is R_{L} the total resistance in the thermocouple circuit is $R_0 + R_{\mathrm{L}}$. The thermo-electric voltage will be $V = S\Delta T$ and the current will be

$$i = \frac{S\Delta T}{R_0 + R_{\mathrm{L}}}.$$

The Peltier cooling is

$$W_{\mathrm{P}} = iST = \frac{S^2T\Delta T}{R_0 + R_{\mathrm{L}}}. \tag{3.6}$$

This cooling is proportional to ΔT, and can be regarded as an additional heat resistance in parallel with the other heat losses of the receiver, given by

$$z_{\mathrm{D}} = \frac{\Delta T}{W_{\mathrm{P}}} = \frac{R_0 + R_{\mathrm{L}}}{S^2T}, \tag{3.7}$$

$${}_{a}z_{\mathrm{D}} = \frac{R_0 + R_{\mathrm{L}}}{S^2}. \tag{3.8}$$

§4. EQUIVALENT CIRCUIT OF A THERMOCOUPLE

If the temperature rise of the receiver of a thermocouple is ΔT, then the voltage generated in the electrical circuit will be

$$V = S\Delta T. \tag{4.1}$$

This relation will be satisfied if we regard the connection between the electrical and thermal circuits of a thermocouple to be a transformer whose "turns ratio" is numerically and dimensionally equal to S. This transformer will give an impedance transformation ratio of S^2 between the two sides of the thermocouple. Equations (3.5) and (3.8) show that this is just the right impedance transformation, provided the "absolute" system is used. We thus arrive at the equivalent circuit for a thermocouple shown in Figure 3.

§5. THE MEASUREMENT OF DYNAMIC IMPEDANCE

The equivalent circuit of Figure 3 shows that ordinary D.C. measurements give the total resistance R_0+R_D of the thermocouple; but the resistance to A.C. of a sufficiently high frequency will be R_0 alone owing to the shunting effect of the thermal capacity of the thermocouple. The value of R_D is then found by subtraction.

A Wheatstone bridge circuit which was found convenient for both the D.C. and A.C. measurements on certain commercial thermocouples is shown in Figure 1. The unusual distribution of resistance between the arms is used in order to obtain maximum sensitivity for a given current through the thermocouple. The effect of ohmic heating is further minimized by repeating the D.C. measurement with the current reversed and averaging the values, which should differ by not more than 10% of R_D. In this way the dynamic resistance can be measured to an accuracy of 1%.

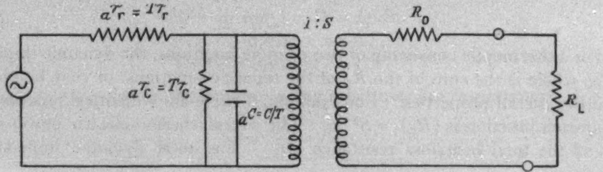

Figure 3. Equivalent circuit of thermocouple.

By applying suitable well-known techniques of A.C. bridge measurement, it is possible to measure both the dynamic impedance and the time constant of a thermocouple. It is not possible to distinguish electrically between heat loss from the receiver due to conduction and due to radiation. The latter may be estimated, however, on the assumption that the receiver is black by using Stefan's law $W=\sigma T^4$, whence

$$r_r = \frac{dT}{dW} = \frac{1}{4\sigma T^3}. \qquad \ldots\ldots(5.1)$$

Putting in numerical values we find

$$r_r \simeq 1{,}500^\circ \text{ c./watt. cm}^2, \qquad \ldots\ldots(5.2)$$

at room temperature. In the Table are given measured values of dynamic resistance, sensitivity u, thermo-electric power, radiation and conduction heat loss resistances etc. of some commercial thermocouples.

Some Characteristics of Three Commercial Thermocouples

u	R_0	n	R_D	$S^{(1)}$	$z^{(2)}$	Receiver area (mm²)	$r_r^{(3)}$	$r_c^{(4)}$	F	$W_{\min}$	η
9·0	105·9	4	4·6	213	5,300	10×0·75	20,000	7,200	20	$14{\cdot}7\times10^{-11}$	1·1
24	115·5	4	8·6	150	20,000	8×0·4	47,000	35,000	15	$5{\cdot}9\times10^{-11}$	3·0
16·5	123·0	4	7·0	180	11,700	8×0·4	47,000	15,600	19	$8{\cdot}7\times10^{-11}$	1·3

u=sensitivity in µv/µw.; F=noise factor in db.; η=relative efficiency of thermocouple (%); other symbols as already used.

(1) Average value for each half junction, $S=R_D/2nTu$; (2) For whole thermocouple, $z=u^2T/R_D$; (3) For whole thermocouple, $r_r=1/4\sigma T^3A$; (4) For whole thermocouple, $\frac{1}{r_c}=\frac{1}{z}-\frac{1}{r_r}$.

§6. THE DETERMINATION OF THERMO-ELECTRIC POWER AND HEAT RESISTANCE

Let the receiver of the thermocouple receive W watts of radiant heat. Then the temperature rise will be $\Delta T = zW$, and the voltage output $V = S\Delta T = SzW$. Therefore the sensitivity of the thermocouple in μv/μw. is given by

$$u = V/W = Sz. \qquad \ldots\ldots(6.1)$$

By solving together equations (3.4) and (6.1) we obtain

$$S = \frac{R_D}{Tu}; \qquad z = \frac{Tu^2}{R_D}. \qquad \ldots\ldots(6.2)$$

Since methods for the determination of u are well known, these relations provide a method of measuring, non-destructively, the values of S and z of a finished thermocouple. The value of S does not necessarily correspond to that of the bulk materials used for the making of the thermocouple, since large changes often take place during the process of manufacture.

§7. SPONTANEOUS FLUCTUATIONS OF TEMPERATURE

It has been shown by Nyquist (1928), that the thermal agitation voltage E_N across resistance R is given by

$$E_N = \sqrt{(4\boldsymbol{k}TBR)}, \qquad \ldots\ldots(7.1)$$

where $\boldsymbol{k}$ = Boltzmann's constant; T = absolute temperature; B = the bandwidth (c/s.) over which the noise is measured.

It follows from Nyquist's thermodynamical reasoning, that this will be true of any passive resistance independent of its physical nature.

Thus across the dynamic resistance of a thermocouple the noise will be

$$E_N = \sqrt{(4\boldsymbol{k}TBR_D)} = S\sqrt{(4\boldsymbol{k}T^2Br)}, \qquad \ldots\ldots(7.2)$$

which corresponds to a spontaneous fluctuation in the temperature of the receiver whose R.M.S. value ΔT_N is given by

$$S\Delta T_N = \Delta E_N,$$

$$\Delta T_N = \sqrt{(4\boldsymbol{k}T^2Br)} = \sqrt{(4\boldsymbol{k}TB_a r)}. \qquad \ldots\ldots(7.3)$$

The generalization of (7.3) to a resistance not grounded at one end is trivial. It may then be regarded as giving the temperature noise in a given bandwidth across any heat resistance r. What is actually observable is the difference in temperature in the two thermal capacities terminating r. But the expression does not involve the capacities because the noise is unaffected by the magnitude of these capacities so long as they are small enough to have no appreciable storage action up to the frequency range comprising B.

In an ideal thermocouple there is no conductive heat loss so that $r = r_r$. The least amount of energy detectable is that producing a temperature rise equal to the spontaneous fluctuations, that is

$$W^\circ_{\min} r_r = \Delta T_N = \sqrt{(4\boldsymbol{k}T^2Br_r)},$$

$$W^\circ_{\min} = \sqrt{\left(\frac{4\boldsymbol{k}T^2B}{r_r}\right)}. \qquad \ldots\ldots(7.4)$$

The value of r_r is given by (5.1) or (5.2). For example, a thermocouple having receiver area $2 \times 0{\cdot}2$ mm² has

$$r_r = \frac{1{,}500 \times 100}{2 \times 0{\cdot}2} = 3{\cdot}8 \times 10^5 \,^\circ\text{c/watt.} \qquad \text{and} \qquad W^\circ_{\min} \simeq 4 \times 10^{-12} \text{ watts}$$

for a bandwidth of 1 c/s. The best thermocouple with this area measured by us has a sensitivity 3×10^{-11} watts for $B = 1$ c/s.

§8. THE ABSOLUTE SENSITIVITY OF A THERMOCOUPLE IN TERMS OF ITS DYNAMIC IMPEDANCE

By absolute sensitivity of a thermocouple we mean the incident radiation $W_{\min}$ that, falling on the receiver, produces unit signal-to-noise ratio in the electrical circuit. For the sake of theoretical uniformity, we take this to mean equality of the signal and the R.M.S. noise, although in practice we find that a signal is not definitely detectable unless it is equal to the peak-to-peak noise, which is about six times larger. We assume that the receiver is perfectly black, and that the noise is due solely to thermal agitation.

Consider first the thermocouple connected to a current detector, such as a galvanometer. Then the R.M.S. noise current in the circuit will be, by (7.1),

$$i_N = \sqrt{\left(\frac{4\boldsymbol{k}TB}{R_0 + R_L + R_D}\right)}. \qquad \ldots\ldots(8.1)$$

To calculate the signal current, we use Thévenin's theorem, which states that any linear generator can be represented by an E.M.F. equal to the open circuit voltage delivered by the generator, in series with an internal impedance.

Let heat energy W fall on the receiver, the thermocouple being open circuited. Then the temperature rise $\Delta T = zW$, and the E.M.F. generated by the thermocouple will be $E_S = SzW$. The total internal resistance of the thermocouple is $R_0 + R_D$, therefore the current when an external load R_L is connected will be

$$i_S = \frac{SzW}{R_0 + R_D + R_L}. \qquad \ldots\ldots(8.2)$$

Putting $i_S = i_N$ we obtain

$$W_{\min} = \frac{\sqrt{[4\boldsymbol{k}TB(R_0 + R_D + R_L)]}}{Sz}. \qquad \ldots\ldots(8.3)$$

Equation (8.3) shows that optimum conditions are obtained when $R_L \ll R_0 + R_D$. In practice, considerations of damping of the galvanometer often lead to this condition being fulfilled.

We write, therefore, in such cases

$$W_{\min} = \frac{\sqrt{[4\boldsymbol{k}TB(R_0 + R_D)]}}{Sz}. \qquad \ldots\ldots(8.4)$$

The Peltier loss appears in the above argument as the drop in voltage across r_D when the thermocouple delivers current. To illustrate this, when the thermocouple is delivering current into R_L, we have by (3.7)

$$\Delta T = W \frac{1}{\dfrac{1}{z} + \dfrac{1}{z_D}} = \frac{W}{\dfrac{1}{z} + \dfrac{S^2T}{R_0 + R_L}}.$$

Therefore
$$V_{\mathrm{S}}=\frac{SW}{\dfrac{1}{z}+\dfrac{S^2T}{R_0+R_{\mathrm{L}}}}.$$

This is not the E.M.F. generated by the thermocouple, but the voltage appearing across R_0+R_{L}, as may be verified by referring to the equivalent circuit. Therefore

$$i_{\mathrm{S}}=\frac{SW}{\left(\dfrac{1}{z}+\dfrac{S^2T}{R_0+R_{\mathrm{L}}}\right)(R_0+R_{\mathrm{L}})}=\frac{SzW}{R_0+R_{\mathrm{L}}+S^2Tz}=\frac{SzW}{R_0+R_{\mathrm{L}}+R_{\mathrm{D}}},$$

which is identical with equation (8.2).

When the thermocouple is connected to a voltage detector, which is assumed to have an infinite impedance, we have

$$E_{\mathrm{S}}=SzW. \qquad \ldots\ldots(8.5)$$

The R.M.S. noise voltage is $E_{\mathrm{N}}=\surd[4\boldsymbol{k}TB(R_0+R_{\mathrm{D}})]$

whence
$$W_{\mathrm{min}}=\frac{\surd[4\boldsymbol{k}TB(R_0+R_{\mathrm{D}})]}{Sz},$$

which is identical with equation (8.4) as it must be according to Thévenin's theorem.

Equation (8.4) is only valid when the speed of response is limited by the amplifier and not by the thermocouple; otherwise the fall in thermocouple output at high frequencies must be considered. Daly (1947) has discussed this case. In comparing thermocouples it is convenient to use (8.4) to reduce the sensitivity to $B=1$ c/s. as a standard condition, which corresponds to an amplifier response time of ¼ sec. This may be done formally even when the thermocouple response is slower than this.

For an ideal thermocouple $z=r_{\mathrm{r}}$ and $R_0=0$, therefore

$$W^{\circ}_{\mathrm{min}}=\frac{\surd(4\boldsymbol{k}TBR^{\circ}_{\mathrm{D}})}{Sr_{\mathrm{r}}}=\sqrt{\left(\frac{4\boldsymbol{k}T^2B}{r_{\mathrm{r}}}\right)},$$

which is identical with equation (7.4).

We define the noise factor F of a thermocouple as the ratio between the minimum detectable energy W_{min} and the corresponding quantity W°_{min} for an ideal thermocouple having the same receiver area. It is conveniently expressed in decibels:

$$\begin{aligned} F(\mathrm{db})&=20\log(W_{\mathrm{min}}/W^{\circ}_{\mathrm{min}})\\ &=10\log\frac{R_0+R_{\mathrm{D}}}{R^{\circ}_{\mathrm{D}}}+20\log\frac{r_{\mathrm{r}}}{z}\\ &=10\log\frac{R_0+R_{\mathrm{D}}}{R_{\mathrm{D}}}+10\log\frac{r_{\mathrm{r}}}{z}. \qquad \ldots\ldots(8.6)\end{aligned}$$

Noise factor is a very convenient measure of sensitivity since it is independent of bandwidth.

Daly (1947) has used (8.6) to show how a thermocouple may be designed for minimum noise factor, which he finds is

$$F_{\mathrm{opt}}\simeq\surd(1+16L/S^2),$$

where $L=\frac{1}{4}(L_1+L_2)+\frac{1}{2}\surd(L_1L_2)$ is an average of the Lorenz numbers L_1 and L_2 for the two thermo-electrics. The noise factor of the thermocouples given in the Table is as low as six times. If the thermo-electric power could be increased to 1,000 μv/°c., the theoretical limit of sensitivity given in equation (7.4) would be practically reached.

§9. COMPARISON WITH PREVIOUS SENSITIVITY FORMULAE

A number of expressions have previously been published for the absolute sensitivity of a thermocouple. The one most frequently quoted is probably that of Cartwright (1934), who gives (in our notation)

$$W_{\min}=\frac{\sqrt{[4\boldsymbol{k}TB(R_0+R_{\mathrm{L}})]}}{S}\left\{\frac{1}{z}+\frac{S^2T}{R_0+R_{\mathrm{L}}}\right\}. \qquad \ldots\ldots(9.1)$$

Assuming $R_{\mathrm{D}} \ll R_{\mathrm{L}}+R_0$ and using (3.4), binomial expansion to first order in $\dfrac{R_{\mathrm{D}}}{R_{\mathrm{L}}+R_0}$ of our formula (8.3) gives

$$W_{\min}\simeq\frac{\sqrt{[4\boldsymbol{k}TB(R_0+R_{\mathrm{L}})]}}{S}\left\{\frac{1}{z}+\frac{1}{2}\frac{S^2T}{R_0+R_{\mathrm{L}}}\right\}. \qquad \ldots\ldots(9.2)$$

Examination of Cartwright's (1934) derivation shows that he has neglected both the noise in R_{D} and the effect of this resistance in impeding the noise current. On balance, the noise current comes out too great, which accounts for the difference between (9.1) and (9.2).

We have shown in §8 how our formulae give equal short- and open-circuit sensitivities. (To avoid any logical circularity the derivation was given both with and without the use of Thévenin's theorem). But according to the derivation of (9.1) this agreement is not obtained, for the Peltier effect, which is represented by the term $S^2T/(R_0+R_{\mathrm{L}})$, is considered to influence only the signal and not the noise. Therefore (as would be expected from the form of the equation) this term vanishes on open-circuit although it occurs in the expression for short-circuit sensitivity.

It may also be verified that if the temperature noise in the receiver is taken into account, but the effect of z_{D} on this neglected, then the open-circuit sensitivity agrees with (9.2), but in the short-circuit formula the numerical factor in the "Peltier term" is 3/2. Such formulae have frequently been proposed to the present author, and are given here in order that the sources of error may be identified.

§10. THE EFFICIENCY OF A THERMOCOUPLE

It will be assumed that the thermocouple is matched to its load, so that the power delivered is a maximum. Equations (8.2) and (8.5) give the short-circuit current and open-circuit voltage:

$$i_{\mathrm{S}}=\frac{SzW}{R_0+R_{\mathrm{D}}}; \qquad V_{\mathrm{S}}=SzW.$$

The maximum power is therefore

$$P=\tfrac{1}{4}i_{\mathrm{S}}V_{\mathrm{S}}=\frac{S^2z^2W^2}{4(R_0+R_{\mathrm{D}})} \qquad \ldots\ldots(10.1)$$

and the energy efficiency

$$\epsilon=\frac{P}{W}=\frac{S^2z^2W}{4(R_0+R_{\mathrm{D}})}. \qquad \ldots\ldots(10.2)$$

This may be written

$$\epsilon = \frac{R_D}{4(R_0+R_D)}\frac{zW}{T} = \frac{R_D}{4(R_0+R_D)}\frac{\Delta T}{T}\left(1+\frac{z}{z_D}\right),$$

since

$$\Delta T = \frac{W}{1/z+1/z_D}.$$

Thus the efficiency is proportional to the input energy, but is a constant fraction of the thermodynamic limit $\Delta T/T$. For an ideal thermocouple $R_0=0$, $z=r_r$, and (10.2) becomes

$$\epsilon^\circ = S^2 r_r^2 W/4R_D^\circ. \qquad \ldots\ldots(10.3)$$

Since the matching condition is here $R_L=R_D^\circ$, the electrothermal heat loss $z_D=r_r$. Therefore

$$\Delta T^\circ = W\frac{1}{1/r_r+1/z_D} = \tfrac{1}{2}Wr_r,$$

$$\epsilon^\circ = \frac{S^2 r_r T}{4R_D^\circ}\frac{Wr_r}{T} = \frac{1}{2}\frac{\Delta T^\circ}{T}. \qquad \ldots\ldots(10.4)$$

Thus, even ideally only half the full thermodynamic efficiency is realized with respect to the energy received. This is because half the incident radiation is converted into electrical power with efficiency $\Delta T/T$, while half is re-radiated by the receiver, as follows from the equality of r_r and z_D.

Comparing (10.2) and (10.3)

$$\frac{\epsilon}{\epsilon^\circ} = \eta = \frac{z^2}{r_r^2}\frac{R_D^\circ}{R_0+R_D} = \frac{z}{r_r}\frac{R_D}{R_0+R_D}. \qquad \ldots\ldots(10.5)$$

The quantity η may be called the relative efficiency. Comparison with (8.6) shows that it is the reciprocal of the square of the noise factor, as it must be from energy considerations.

ACKNOWLEDGMENTS

As already stated, relations equivalent to (7.3), (7.4) and (8.4) were first given by Milatz and Van der Velden (1943). They have since been derived, apparently independently, by Daunt (1945), Golay (1947) and Jones (1947). All these authors use the Einstein formula $\overline{\Delta E^2} = \boldsymbol{k}T^2(dE/dT)$. Lewis (1947) has deduced the noise in a radiation resistance from the statistics of radiation. Golay (1947) has also given a equivalent circuit differing from that presented here.

Our gratitude is due to Dr. G. B. B. M. Sutherland for inspiration and encouragement throughout the time that the author was working in his laboratory during this investigation.

It is a pleasure to record our thanks to Dr. E. F. Daly for many valuable and stimulating discussions. Our thanks are also due to the Admiralty for permission to publish this work.

REFERENCES

Cartwright, C. H., 1934, *Z. Phys.*, **92,** 153.
Daly, E. F., 1947, *Thesis* (Cambridge University), and private communications.
Daunt, H., 1945, *Admiralty Report C.L. Misc.* 52 (unpublished).
Golay, M., 1947, *Rev. Sci. Instrum.*, **18,** 347.
Jones, R. C., 1947, *J. Opt. Soc. Amer.*, **37,** no. 11, p. 879.
Lewis, W. B., 1947, *Proc. Phys. Soc.*, **59,** 34.
Milatz, J. M. W., and Van der Velden, H. A., 1943, *Physica*, **10,** 369.
Nyquist, H., 1928, *Phys. Rev.*, **32,** 110.

Some Experiences in the Application of the Electron Microscope to the Study of Steels

By F. W. CUCKOW and J. TROTTER

Communication from the National Physical Laboratory, Teddington, Middx.

MS. received 11*th January* 1949; *read at Science Meeting at Manchester* 9*th December* 1948

ABSTRACT. Steel specimens have been examined with light and electron microscopes. The replica technique has been used for the electron microscope work, and all the specimens have been studied with both " Formvar " plastic and polystyrene-silica replicas. The micrographs are critically examined and compared.

There is an obvious gain in picture sharpness in the electron micrographs, particularly in those from silica replicas. It is found, however, that interpretation of the micrographs from plastic replicas in terms of the geometry of the specimen surfaces is more straightforward.

---

§1. INTRODUCTION

The electron microscope is now firmly established as an instrument capable of resolving object details beyond the power of light or ultra-violet microscopes.

Practical experience has shown that object details with a spacing of about 10 A. can be clearly resolved in special circumstances, and the attainment of such resolving powers is in accordance with the predictions of theory based on the effective wavelength of the moving electrons and the aberrations present in electron lenses.

Resolution of object details spaced 10 A. apart implies a real magnification of 100,000 diameters, but it must be emphasized that magnifications of this order can be obtained with ideal objects only, such as minute crystals of a heavy metal which cause an appreciable degree of electron scattering in spite of their small size. This scattering of electrons by the particles leads to their becoming visible in the electron microscope and, once made visible, the high resolving power of the microscope is shown by its ability to reproduce closely spaced particles in the object as clearly separated features in the highly magnified image.

The high resolving powers mentioned above have been attained by means of the *transmission* type of electron microscope, closely parallel in form to the *transmission* type of light microscope as distinct from the *metallurgical* light microscope in which the image is formed by light reflected from the specimen. The metallurgical light microscope suffers no loss in resolving power through the use of reflected light, but this is not true of electron microscopes working with reflected electrons. The resolving power of the latter is still relatively poor, and the best electron metallography has, therefore, been carried out on transmission type electron microscopes through the agency of replicas of the surfaces of the metal specimens.

In spite of the limitations set by this indirect method of working, the resultant electron micrographs of metal specimens show finer detail than corresponding photomicrographs, and an attempt has been made in the work here reported to take advantage of this improvement in picture sharpness in seeking for information unrevealed by normal metallurgical microscopes employing light.

Two types of steel sample have been examined.

The first provides a direct test of the reputed gain in resolving power of electron microscopes. From considerations of its constitution and history, aided by examination on a light microscope, the sample was considered to consist of "acicular ferrite and unresolved pearlite in a martensitic matrix". The primary aim of the electron microscopical examination was to determine if there was in fact a fine pearlitic structure present.

The second type of sample was a steel showing "intermediate transformation products". It was hoped that the electron micrographs would provide additional information on the nature of these transformation products.

§ 2. MATERIALS USED IN THE EXAMINATIONS

(*a*) *Chromium steel*: "*unresolved pearlite*". The first sample, identification No. X3, was a chromium steel of the following composition: C 0·83%, Si 0·28%, Mn 0·82%, Ni 0·34%, Cr 1·13%, Mo 0·05%.

The specimen examined had been cut from a Jominy bar used in assessing the hardening characteristics of the steel. Full metallurgical details are given by Pumphrey and Jones (1946). A Jominy bar is a steel bar approximately 4 in. (10 cm.) long × 1 in. (2·5 cm.) diameter which is heated to the hardening temperature and quenched by directing a standard jet of cold water against one end. Points along the bar cool at different rates, and the present specimen was taken at a point 1·4 in. (3·5 cm.) from the quenched end, where the rate of cooling was such as to produce small masses of "unresolved pearlite" in a matrix of martensite.

(*b*) *Nickel-chromium steel*: "*intermediate transformation products*". The second material was a nickel steel to specification 4S11. Chemical analysis gave the following results: C 0·27%, Ni 2·81%, Cr 0·99%, Mo 0·35%.

Three samples had been prepared, each being in the form of a 90° sector of a short cylinder approximately 2 cm. in diameter and 3 mm. in length. These were heated at 900° c. for 15 minutes in a pot of cast iron chips and then put into a lead bath maintained at 444° c.; sample No. 305 was immersed for 20 seconds, No. 303 for 1 minute and No. 302 for 5 minutes. After these varying periods in the bath, they were removed and quenched in water at room temperature.

When quenched in this manner in a lead bath, the steel undergoes a slow transformation whereby a constituent known as the "intermediate transformation product" is formed. Small masses of this constituent appear after a few seconds and increase in quantity until, after five or ten minutes, the majority of the steel has been converted to the new form (Griffiths, Pfeil and Allen 1939).

Each sample was mounted in bakelite in the normal manner, being subjected in the process to temperatures rising from room temperature to 200° c. over a period of perhaps 20 minutes, followed by a further period of 4 minutes at 200° c. and subsequent return to room temperature over a further period of perhaps 20 minutes.

§ 3. PHOTOMICROGRAPHY OF THE SPECIMENS

The specimens were all polished in the normal manner and etched in nitric acid in alcohol. Photomicrographs were prepared on a Vickers Projection Microscope using a 2 mm. objective under oil immersion and Ilford Chromatic Plates.

§4. REPLICA PROCESSES

(i) *Plastic Film Replicas*

The plastic film replica method was initiated by Mahl (1940) who used nitrocellulose as a film-forming material. This has now largely been supplanted by polyvinyl formal ("Formvar") which gives a very much stronger film and so facilitates detachment from the metal specimen (Schaefer and Harker 1942). The replica films normally used are perhaps 500 to 1000 A. thick in the thickest parts, i.e. two to four millionths of an inch in thickness, and it will therefore be realized that the films need to be made of a strong material to withstand the stresses set up in detaching them from the metal.

After etching, the specimens were rinsed free of reagent with alcohol, washed in running water, rinsed again with alcohol and then dried with a freshly laundered cloth. Immediately after this drying they were dipped face downwards in a 0·5% solution of "Formvar" in dioxan, and then allowed to drain and dry in a vertical position in a calcium chloride desiccator. In more recent work chloroform has replaced dioxan, as the effects of water vapour present in the atmosphere are less troublesome.

The plastic film was then strengthened by coating it in a similar manner with a film of nitrocellulose obtained from a 2% solution of nitrocellulose in isopropyl acetate. The composite film was detached from the specimen by manipulation under water with a needle and carefully adjusted forceps and brought to the water surface with the backing film of nitrocellulose uppermost. The film was then lifted off the water surface on fine metal mounting grids brought up from below. The whole was carefully dried and then immersed in amyl acetate to remove the nitrocellulose backing. Only after immersion for a period of days is there any obvious damage to the replica. The films were finally rinsed in fresh amyl acetate and then dried in air. They were then ready for examination in the electron microscope.

Each of the specimens used in the present work was treated in this manner.

(ii) *Silica Film Replicas*

Another replica-forming technique is that devised by Heidenreich and Peck (1943). In this case a first cast is made with polystyrene which is moulded against the metal specimen under heat and pressure in an ordinary metallurgical mounting press. When cold, the polystyrene cast is detached from the parent metal and the working face is given a thin coat of silica applied by evaporation *in vacuo*. An apparatus has been devised in which the thickness of the deposited silica film is observed by an optical interference method during the evaporation, and the process may therefore be stopped when the desired thickness has been obtained. The silica film is then detached by solution of the polystyrene in a suitable medium and is mounted on the usual fine metal grids ready for examination in the electron microscope. Successful operation of this technique depends upon close attention to a number of details. These have already been dealt with extensively in the literature and will not be discussed here (Heidenreich and Peck 1943, Barrett 1943, Gerould 1947).

Supplies of the polystyrene used by Heidenreich and Peck were obtained and this material was found to be relatively free from the "crazing" effect and was therefore used in all subsequent work. The handling of the silica replicas was facilitated by a convenient arrangement which has been described in the *Handbook of Electron Microscopy*, edited by D. G. Drummond.

§5. ELECTRON MICROSCOPICAL EXAMINATION OF THE REPLICAS

The replicas prepared in the present work have all been examined on a Siemens-Halske electron microscope which has electromagnetic lenses and has been operated at about 60 kilovolts.

It has been thought desirable to obtain micrographs of relatively large areas of the specimens, and the electron microscope has therefore been operated at a low magnification, generally 1,000 diameters.

§6. RESULTS

(i) *Chromium Steel: "Unresolved Pearlite"*

Figure 1 shows a photomicrograph prepared from sample No. X3. The dark area was considered to consist of unresolved pearlite, but only a suggestion of a lamellar structure can be seen in the photomicrograph. (For all Figures see Plates facing p. 364.)

The picture sharpness shown in the electron micrographs is far superior to that of the photomicrographs. It is still necessary to assess, however, the trustworthiness of the finer detail revealed by the greater sharpness. The electron micrograph from a plastic replica shown in Figure 2 provides clear evidence that a considerable gain in resolving power is being obtained through the use of the electron microscope. The clear evidence of lamellar structure, confirming a prediction made from other considerations, encourages confidence in picture details, and some neighbouring lamellae, clearly shown as separate entities in the electron micrograph, are so closely spaced that they could not be resolved on a normal light microscope. The electron micrograph from the silica replica (Figure 3) on the other hand retains a very high degree of picture sharpness but does not give a clear indication of a lamellar structure.

Both plastic film and silica film replicas show evidence of the structure in the martensitic background areas, including in each case the clear round areas, which appear always light in both martensitic and pearlitic areas. These are probably carbides.

It may be pointed out that some of the coarser parts of the pearlite structure shown in Figure 2 are of such a spacing that resolution by means of an optical microscope might reasonably be expected, but no clear detection of a pearlitic structure has been so obtained.

(ii) *Nickel-Chrome Steel: "Intermediate Transformation Products"*

Figures 4, 7 and 10 show photomicrographs prepared from samples 305, 303 and 302 respectively at a magnification of 900 diameters. A progressive separation of the "intermediate transformation product" is made obvious by the electron micrographs from the plastic film replicas, Figure 5, 8 and 11. All the electron micrographs, both from plastic film and silica replicas, show a great gain in picture sharpness over the photomicrographs, and there are other distinct differences.

The electron micrographs from plastic film replicas show a high degree of photographic contrast between the "intermediate transformation product" areas and the general martensitic background. The geometric nature of the steel specimen's surface can be deduced with a considerable degree of confidence from such micrographs. The dark areas in the electron micrographs correspond to depressed areas on the surface, and light parts correspond to heights. Thus the martensitic areas are relatively flat and only slightly relieved by acicular crystals, but on approaching an "intermediate transformation product" area a ridge is encountered first. There is then a sharp fall into the "intermediate transformation product" area which is in general again very flat. It is, however, relieved by randomly placed peaks (the white dots in the micrographs) which rise at least to the height of the ridge mentioned previously. At the far side of the "intermediate transformation product" area there is again a ridge before the martensitic area is reached.

Such an analysis has particular reference to Figure 8, but the ridges tend to disappear in the case of the specimen showing an advanced stage of the separation (Figure 11); it may be noticed further that the acicular crystal formation is also missing from the last figure. This may be because the specimen photographed in Figure 11 was more lightly etched than that shown in Figure 8.

The marked difference, apart from increased picture sharpness, between the photomicrographs and electron micrographs from plastic replicas is the gain in contrast between the various phases, which has been shown above to be due to their characteristic variations of surface level, which are in turn dependent upon differential etching rates. The constituent giving rise to the white "peaks" within the "intermediate transformation product" has not previously been revealed with the same clearness, although claims have been made that the "intermediate transformation product" contains particles of carbide which are regarded as having been precipitated from supersaturated solid solution in the intermediate product. It is not yet possible to say whether the "peaks" are in fact carbide, martensite or residual austenite, though their general appearance suggests that in many cases they are not identical with the martensite forming the matrix of the steel.

Turning to the electron micrographs from silica replicas, the increase in picture sharpness over the light work is again marked, but the convenient contrast between phases shown by the other electron micrographs is to a large extent lost, although Figure 9 does show something of the same effect.

The detailed inner structure of the "intermediate transformation product" areas shown in the plastic film replicas may indeed be indicated in some of the silica film replicas, but it is considered impossible to give a detailed analysis of that structure from the silica work.

The photomicrographs of these specimens illustrate the difficulty of distinguishing between the phases present when using a normal light microscope, and the general comparison of these various micrographs brings out the point that increase in picture sharpness is not the only line af advance open in metallurgical microscopy, and that it is in fact highly desirable that the general question of visibility of details as distinct from the resolution of closely spaced details be fully examined.

§7. CONCLUSIONS

The overall impression gained in this intercomparison of micrographs is one of undoubted gain in picture sharpness in the case of the electron micrographs with, probably, greatest picture sharpness from silica film replicas. Owing to the difficulties of interpretation of the silica film replicas, however, greatest reliance is placed upon electron micrographs from plastic film replicas since it is believed that these can be interpreted fairly accurately in terms of the geometric structure of the specimen's surface, and this, after all, is the only aim which microscopy

Chromium Steel: " Unresolved Pearlite ".

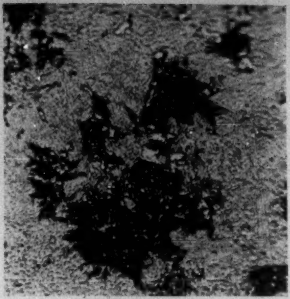

Figure 1. Photomicrograph. × 1,200.

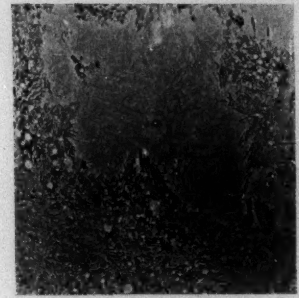

Figure 2. Electron micrograph.
Plastic film replica. × 1,800.

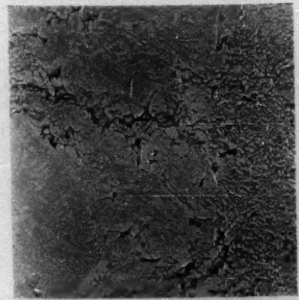

Figure 3. Electron micrograph.
Silica replica. × 1,800.

Nickel-Chrome Steel : " Intermediate Transformation Product ". 20 seconds at 444° C.

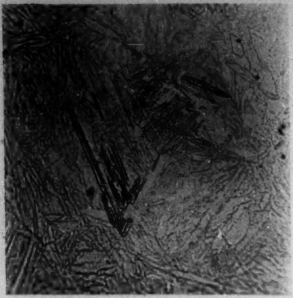

Figure 4. Photomicrograph. ×900.

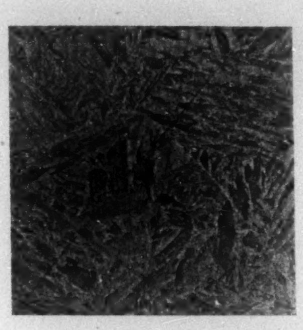

Figure 5. Electron micrograph.
Plastic film replica. ×1,800.

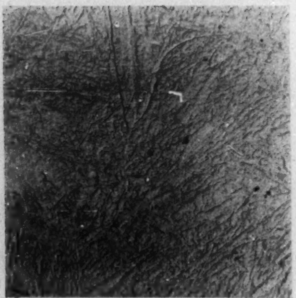

Figure 6. Electron micrograph.
Silica replica. ×1,800.

Nickel-Chrome Steel : " Intermediate Transformation Product ". 1 minute at 444° C.

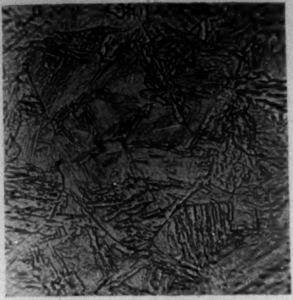

Figure 7. Photomicrograph. × 900.

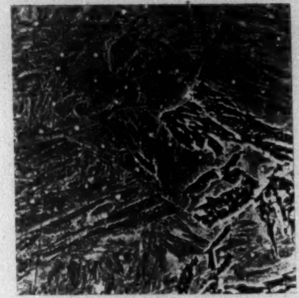

Figure 8. Electron micrograph.
Plastic film replica. × 1,800.

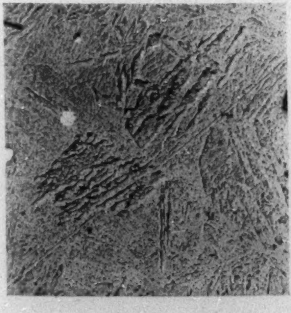

Figure 9. Electron micrograph.
Silica replica. × 1,800.

Nickel-Chrome Steel: "Intermediate Transformation Product". 5 minutes at 444° C.

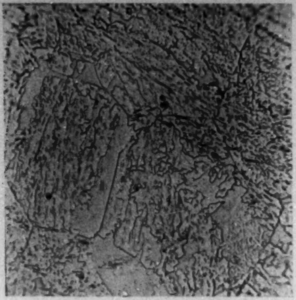

Figure 10. Photomicrograph. ×900.

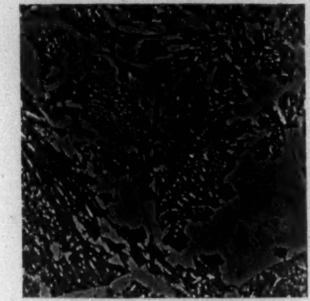

Figure 11. Electron micrograph. Plastic film replica. ×1,800.

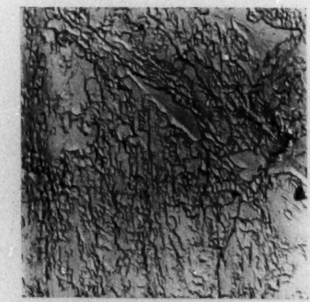

Figure 12. Electron micrograph. Silica replica. ×1,800.

by the use of replicas can have. This view is substantiated by recently published work on the application of the phase contrast microscope to metallurgy (Cuckow 1949). It should be pointed out that difficulty has been experienced in obtaining consistent results from the silica replica process as compared with the relative certainty of the plastic film replica process. There are also objections to the heat and pressure method of silica replica preparation.

The statement that the geometric form of the specimen's surface can be deduced from the plastic film replicas is equivalent to saying that the general replica method is sensitive to variations in the surface level of the specimen and is a means of assessing those relative surface levels.

The distinction between gain in contrast or visibility and gain in resolving power must be emphasized. In some problems it may be adequate to render certain features clear to the eye by a device which does not necessarily involve increased resolving power. The electron microscope in some cases offers this gain in contrast or visibility, coupled with an undoubted gain in resolving power, but is handicapped by an indirect method of working calling for the use of replicas which consume time and make "scanning" of the specimen difficult.

It was pointed out in § 6 (i) that the spacing of some of the pearlite lamellae (Figure 2) was such that resolution on a light microscope might be expected but had not been observed. This may perhaps be a case where the normal light microscope fails to render the lamellae visible by contrast with their background, so that the adequate resolving power of the microscope is not called into play.

ACKNOWLEDGMENTS

The work described has been carried out as part of the research programme of the National Physical Laboratory, and this paper is published by permission of the Director of the Laboratory.

REFERENCES

Barrett, C. S., 1943, *Metals Tech.*, Tech. Publ. 1637.

Cuckow, F. W., 1949, *J. Iron & Steel Inst.*, **161**, 1.

Gerould, C. H., 1947, *J. Appl. Phys.*, **18**, 333.

Griffiths, W. T., Pfeil, L. B., and Allen, N.P., 1939, *2nd Report, Alloy Steels Research Committee*, p. 343.

Heidenreich, R. D., and Peck, V. G., 1943, *J. Appl. Phys.*, **14**, 23.

Mahl, H., 1940, *Z. Tech. Phys.*, **21**, 17.

Pumphrey, W. I., and Jones, F. W., 1946, *Iron and Steel Institute Hardenability Symposium*, Special Report No. 36.

Schaefer, V. J., and Harker, D., 1942, *J. Appl. Phys.*, **13**, 4, 27.

Electrode Ionization Processes and Spark Initiation

By F. LLEWELLYN JONES
Department of Physics, University College of Swansea

MS. received 14*th October* 1948; *in amended form* 18*th January* 1949

ABSTRACT. Spark time lags in short gaps with tungsten electrodes were measured for different degrees of oxidation and activation, and the distributions of lags examined and compared. The results, which showed a reduction of mean lag and a narrowing of distribution following oxidation and activation, are discussed in relation to the mechanism of electron emission from oxidized cathodes for impulse and static conditions, and also for the Geiger counter.

---

§1. INTRODUCTION

The study of spark breakdown in short gaps is of considerable interest from both the fundamental and the technical points of view. In the first place, the phenomenon of spark breakdown is less complicated in short gaps than in long gaps, on account of the smaller influence of the various processes which are believed to attend streamer propagation in long sparks (Loeb and Meek 1941, Teszner 1946); in short gaps the electrodes themselves exert an important influence both on the initiation of the spark and on the subsequent breakdown. In the second place, short spark gaps have important practical applications in electrical engineering (e.g. electrical ignition). For these reasons experimental data concerned with spark gaps of the order of 0·5 mm., which pass maximum spark currents of the order 100 amp. at gas densities corresponding to pressures from about ½ to 3 atmospheres, are of considerable interest. The present investigations were undertaken to examine the influence of the state of electrode surfaces on the actual initiation of the spark, and so to obtain data about the mechanisms of electron production at cold oxidized metal surfaces in a gas under an electric field (Llewellyn Jones 1946).

Comparisons of the ionization produced at various electrode surfaces can be obtained from a knowledge of spark time lags obtained with those surfaces. In most previous measurements of spark lag (vide Thomson and Thomson 1933, Loeb 1939, for references) an approximately constant E.M.F. was maintained across the gap before breakdown; but considerable information about initial electron production may also be obtained by the simple method of measuring the potential difference at which a gap breaks down on a rising wave-front of E.M.F., since the greater the time lag in the production of the initial electron the higher the potential difference. Under certain conditions the time delay before breakdown occurs may be deduced approximately from measurements of the sparking potentials with both static and impulsive applied E.M.F., provided that the rate of rise of the E.M.F. pulse is known. In this way the production of electrons at various electrode surfaces was compared for sparks in air and in nitrogen at pressures from about 50 cm. Hg to about 3 atmospheres. Some of the experimental work described below originally formed part of a research programme on fundamental problems of the electrical ignition of aero engines, and was carried out early in the war.

§ 2. EXPERIMENTAL PROCEDURE

The principle of the method employed for measuring spark time lag with a pulse of E.M.F. such as that of Figure 1 (*a*) (see Plate) is as follows. The value of the static breakdown potential V_s is attained at a time t_0, but if the spark initiation and breakdown mechanism with the particular pulse involve a time lag t, on impulse breakdown the spark will occur at a higher potential V_1 at the later time t_1, where $t = t_1 - t_0$. If V_s and V_1 are measured, then $t_1 - t_0$ may be calculated from the slope of the E.M.F.–time curve.

The total spark lag is made up of two parts: the initiatory (statistical) time lag, which is the interval required for the appearance of adequate pre-breakdown ionization, and the formative time lag, which depends on the time taken for the actual spark mechanism to develop from the initial ionization to complete breakdown. For long sparks at high pressures this formative time is, at most, of the same order as the transit time for electrons, and it may even be less (Teszner 1946); at low pressures of $\frac{1}{2}$ atmosphere or lower the time lag may be as high as the transit time for positive ions. Assuming the drift velocity of the electrons to be about $1{\cdot}7 \times 10^7$ cm/sec. and that of the positive ions to be of the order of 10^5 cm/sec. (Thomson and Thomson 1933), the transit times for short gaps of about 0·3 mm. are of the order $1{\cdot}7 \times 10^{-9}$ sec. and 3×10^{-7} sec. respectively, so that a time lag of about 10^{-9} sec. can occur at these low gas pressures even when statistical lag is eliminated by adequate initial ionization. On the other hand, statistical time lags resulting from the normal processes of pre-breakdown ionization are much greater than this value, and are, in fact, of a different order of magnitude. The chance of producing electrons suitably placed for leading to breakdown will increase with the volume of the gap; in short gaps with a gas volume of, say, only 0·14 cm^3 the initial gas ionization is very low, and long statistical time lags of the order of 10^{-4} sec. may be expected (Cobine and Easton 1943) if no other source of ions exists. Thus, in a study of pre-breakdown ionization in gaps of small volume the time lags to be measured will lie within the range 10^{-6} sec. to 10^{-4} sec. or greater, rather than within the range 10^{-7} sec. to 10^{-9} sec.

In this method of deducing the time lag from the values of the static and impulsive pre-breakdown potentials, it is thus necessary that time spark delays of the order 10^{-6} sec. should produce measurable changes in the breakdown potential. Suppose the static sparking potential of 3·0 kv. is measured on a cathode-ray oscillograph by producing a vertical deflection of, say, about 15 mm. If the smallest potential on impulse breakdown which can be easily measured on the oscillograph (by giving a deflection of, say, 15·5 mm.) is 3·1 kv., and if this is to represent the smallest time lag significant in this study (say 10^{-6} sec.), then the linear rate of rise of E.M.F. in the pulse applied to the gap must be 10^5 kv/sec. Pulses of E.M.F. of this kind can readily be attained from thermionic valve circuits, but a simple method is to use a standard aero-engine magneto * modified by reducing the number of turns on the secondary coil from about 10,000 to about 1,000 or 3,000. By this means the rate of rise of E.M.F. can be made sufficiently fast for the present experiments even when feeding a condenser of about 10,000 pF. for discharge through the spark gap; in this way a pulse of which the initial part is practically sinusoidal was obtained. A typical pulse is shown in Figure 1 (*a*). With such pulses a peak voltage of about 4 kv. can be attained in about 10^{-4} sec., and a rise of voltage of 3·0 kv. requires about 5×10^{-5} sec.

---

* A magneto was used in these experiments because of its practical application.

The spark circuit is illustrated in Figure 2, where L_1 is the secondary coil of the magneto M, C the spark reservoir condenser ($\simeq$10,000 pF.), which also controlled the amplitude of the pulse, and G the spark gap. By altering the speed of the magneto, recurrent pulses could be produced at rates from about 50 pulses/sec. to 400 pulses/sec.

In former studies of spark lags by Tilles (1934) and Cobine and Easton (1943), the electrodes consisted of small metal spheres. In the present experiments it was considered advisable to use a uniform field, and parallel plates were employed; the electrodes consisted of tungsten discs, $\frac{1}{2}$ inch in diameter, spot-welded or brazed to $\frac{1}{8}$ inch or $\frac{3}{32}$ inch tungsten rods, and the sharp edges of the faces of the discs were ground off before assembling. These were supported by sealing them in a hard glass tube about 2 inches long, and tubes were constructed with various gap distances from 0·25 mm. to 0·5 mm. While most of the experiments were done with nitrogen at atmospheric pressure, others were carried out with air and with oxygen at various pressures. The nitrogen was commercially produced and contained 0·5% oxygen. When a pulse similar to that of Figure 1 (*a*) was applied to the gap, breakdown was followed by an arc, but the gap was designed so that the arc extinguished after a few microseconds. Consequently, the E.M.F. across the gap rose again, and in some cases another breakdown occurred, generally at lower voltage, because of the ionization remaining in the gap. This effect is illustrated in Figure 1 (*b*) for two successive pulses nearly superposed. The time scale is indicated by a 5 kc/s. trace.

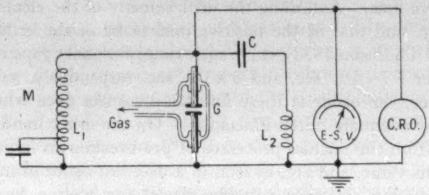

Figure 2. The spark circuit.

In addition to the measurements of the breakdown voltage on a thermionic electrostatic peak voltmeter, the deflections obtained on an oscillograph were photographically recorded on a moving film. No time-base was used, so that all voltage deflections occurred in the same vertical line, which was then of varying density, due to the E.M.F. in the pulse after breakdown, as shown in Figure 1 (*b*). The breakdown voltage is given by the length of the maximum deflection; successive pulses were of alternate polarity, so that vertical deflections gave lines on the film both above and below the line of zero voltages. The rate of recurrence of the sparks and the speed of the film were so adjusted that two breakdowns could be distinguished; typical records are given in Figures 3 (*a*), (*b*), for sparking rates of 15 and 150 sparks/second.

To obtain the maximum control over the discharge conditions, the peak values of breakdown currents in the gap were controlled by varying the electrical constants L_2 and C in the circuit containing the gap, where L_2 is a series inductance. For a given energy from the E.M.F. pulse, the peak breakdown current is inversely proportional to the sparking potential. Various peak currents from 80 amp. to 200 amp. were used by controlling the gap voltage and the natural oscillation frequency of the spark circuit (Llewellyn Jones 1945).

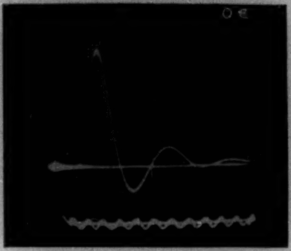

Figure 1 (*a*). The E.M.F. pulse.

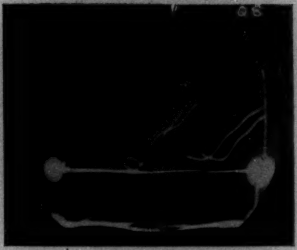

Figure 1 (*b*). Double breakdown.

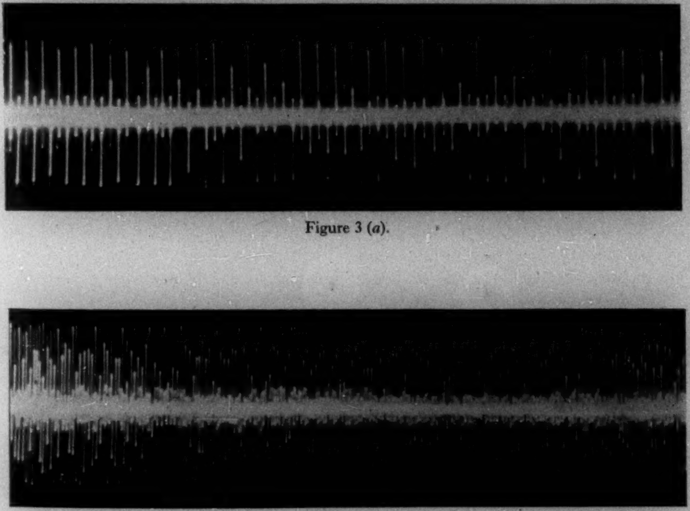

Figure 3 (*a*).

Figure 3 (*b*).

Figure 3. The distribution of spark voltages.

§ 3. RESULTS OF SPARK LAG MEASUREMENTS

The relation of sparking potential to the statistical time lag will now be considered. The formative time lag is of a much lower order of magnitude than the statistical lag in short gaps, so that the total time lag is almost entirely due to the statistical lag alone. The statistical lag is not however fully determined by the time interval between the appearance of successive electrons in the gap, because it will also depend on (*a*) the actual location of the electron along the gap length, and (*b*) the value of the electric field at the moment the electron appears. It is clear that, at any given voltage, an electron which appears near the anode has the least probability, while one which appears near the cathode has the greatest probability, of leading to breakdown. Further, since the gap voltage increases with the time lag, it follows that electrons which appear later on in the lag interval have a greater chance of leading to breakdown than those which appear early in the interval, and this fact would tend to reduce the average time lag. Thus in investigating the reduction of the spark lag due to enhanced production at or near the cathode surface, it is first necessary to determine the value of the average time lag which corresponds only to the currents due to natural volume processes of pre-breakdown ionization (cosmic rays, radioactivity) and to other processes such as the break-up of gaseous negative ions, ionization by high energy metastable atoms, cathode emission due to emission of positive ions or of metastable atoms in the pre-breakdown ionization currents across the gap.

For these purposes a typical spark gap circuit with a static breakdown potential of 1·8 kv. mm. was set up, and pulses of 3·6 kv. peak were applied at a rate of 260 pulses/sec. At first the impulse breakdown voltage was not much greater than the static value, but after a few minutes the breakdown voltage began to rise, and the effect was clearly seen on the peak voltmeter or on the cathode-ray oscillograph. After longer periods of about 50 minutes the peak voltage rose to values higher than 3·6 kv., and the gap could only be broken down with a pulse voltage greater than twice the static value: the corresponding time lag was 10^{-4} sec. or longer. These recorded lags were not statistically distributed because the majority of the lags were greater than the time interval (10^{-4} sec.) used in the recordings; to have recorded a statistical distribution, the applied E.M.F. would have had to be maintained constant for about 10^{-3} sec., and such pulses were of little interest in this work.

After the initial sparking, the electrode surfaces had been considerably smoothed by the action of the sparks, and it was observed that these surfaces gave rise to long time lags: but, when the electrodes had been roughened by the heat used in their construction, low statistical lags were obtained. When the electrodes were clean and smooth and the spark lags were all high, the effective processes of initial ionization were only those mentioned above, namely, the spatial gas processes together with any cathode emission resulting from the pre-breakdown Townsend currents. The efficiency of all these processes is known to be low, and the long time lags were indicative of the low efficiency of electron production by these processes even when over-voltages of 100% were applied. This result shows that in spite of the high probability of an electron leading to a spark at such a high over-voltage, the initiatory time lags were still of the order of 10^{-4} sec.; so that it must be concluded that within times $\geqslant 10^{-4}$ sec. the production of electrons in the gap from natural processes was negligible.

The first experiments were carried out with tungsten electrodes in air at atmospheric pressure, and it was soon found that after the initial sparking phase, in which the electrodes were rendered inactive, and consequently long time lags occurred, a phase of greater electrode activity set in. In fact, the longer the sparking continued and the longer the electrodes were exposed to air, the more active they became, and this was indicated by a reduction in the magnitude of the time lags. The reduction is well illustrated by plotting the number of sparks against the time lag.

In the E.M.F. pulse given in Figure 1 (*a*), a large part of the wave-front is practically linear with the time, and when the sparks occur on this linear section the spark lags are proportional to the over-voltage. Typical results are given in Figure 4, where the number of breakdowns (i.e. time lags) is plotted against the times (deduced from the over-voltages obtained from Figure 3). Curve A is a set of 403 spark lags giving their distribution about the mean value ($\simeq 20\,\mu$sec.) for oxidized tungsten electrodes in an advanced state of activity. Curve B represents an equal number of lags obtained with comparatively inert, slightly oxidized electrodes. Curve C, in the inset, represents part of a set of lags obtained with smoothed electrodes. Although their shape was affected by the shape of the E.M.F. pulse used, the curves clearly show how, as electrode activity increased, marked reductions in the mean time lags from approximately 10^{-4} sec. to 20 μsec. were produced.

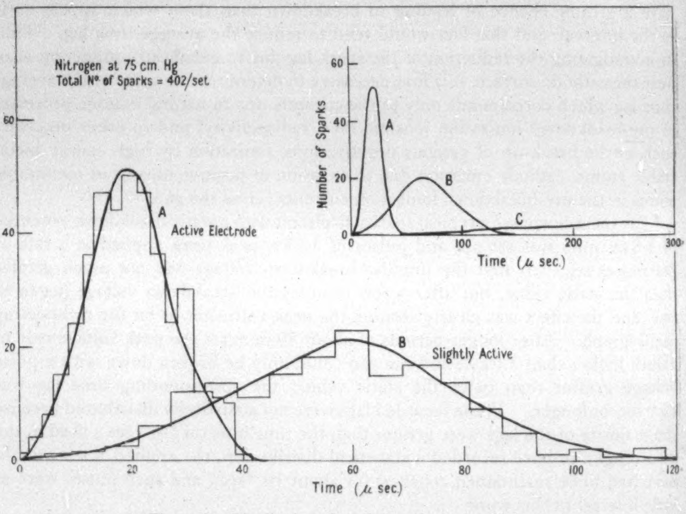

Figure 4. Distribution of spark lags about mean lag.

Experiments were carried out with air, oxygen, and nitrogen, and at pressures lower and higher than atmospheric. In general, it was found that the mean time lags increased as the gas pressure was reduced, and that they were greatest for oxygen and least for nitrogen: in fact, time lags as low as 6 μsec. were recorded in that gas. The longer lags in oxygen were no doubt due to the influence of electron attachment, by which electrons could be removed from the current by the formation of heavy negative ions.

It is clear that the reduction in the time lags of sparking must have been caused by an increased rate of ionization, produced in some manner by the activation of the electrodes due to prolonged sparking in air. It is now necessary to consider the various processes by which this can occur.

§4. EFFECTS OF ELECTRODE ROUGHNESS

It is well known that roughness of a cathode surface reduces the statistical spark lag (Thomson and Thomson 1933), and the mechanism is usually considered to be field emission due to the concentration of electric field at microscopic points produced by the roughening. The reduction in sparking potentials and initial ionization observed by Howell (1939) were attributed to a roughness of the electrode surface, but no polarity effect was observed, i.e. short time lags and lowered sparking potential could be obtained even when the anode alone was rough. It follows that the cause, at least in part, of the short lags in Howell's observations could not have been due to electron emission from the rough electrode, but must then have been due to some effect in the gas. A possible effect would have been photo-ionization of the gas in the gap by the radiation emitted from minute corona discharges occurring at microscopic points on the rough electrode, and such discharges might well have occurred when the rough surface was either anode or cathode, as they would depend on the electric field only.

Support for this view is obtained by the fact that under certain conditions in the present experiments a pre-breakdown corona could be seen over an electrode which had been used for a very large number of sparks, and a heavy pre-breakdown current of some microamperes to milliamperes was passed. In many cases these corona discharges, or electrode glows, imposed so heavy a load on the magneto pulse generator that the E.M.F. applied to the gap was reduced below the normal static sparking value, and a spark could not be obtained. In order to obtain further information about these particularly active electrode surfaces they were examined micro-photographically at magnifications up to 500. It was found that certain parts of the oxidized electrode stood out to distances of approximately 10^{-3} cm.; further, on some parts, minute spikes were seen to project through the oxidized surface, and on other parts spikes were found on the clean metal: these surfaces had been heavily sparked. It was noticed that those electrodes which showed pronounced pre-breakdown corona had a number of spiked projections. Such projections would be most effective for irradiating the gas independently of the polarity, and it would appear that this phenomenon strongly supports the view that roughened electrons produce spatial ionization by irradiating the gas from corona discharges at minute projections where the field is concentrated.

§5. SOME PROPERTIES OF OXIDIZED CATHODES

Low time lags observed with the first group of sparks in a new tube were in all probability due to the rough surface of the electrode, produced by the heating used in the construction of the tube. Similar effects have been recorded by Howell (1939) and Cobine and Easton (1943). After passing through the state of inactivity (presumably due to the smoothing of the surfaces), continued sparking and rest in air produced a state of activity on the electrodes. These then appeared to be covered with a grey layer, which visual examination showed to be a mixture of the yellow and dark blue oxides of tungsten. In order to separate anode effects from cathode processes a polarity test was employed; and when successive pulses of E.M.F. with the same polarity were used, low time lags were obtained when the oxidized electrode was the cathode, and a smoothed clean electrode was the anode. On the other hand, when the clean tungsten electrode was made the cathode and the oxidized one the anode, long time lags occurred; consequently, it follows that the oxide layer on the cathode was able to produce enhanced initial ionization.

It is important to investigate whether this enhanced ionization was due to an inherent property of the oxide, or was merely due to the geometry of the oxidized surfaces (i.e. giving rise to corona because of its roughness). To test this point, tungsten electrodes were constructed and were oxidized, not by sparking and exposure to air, but by treatment with nitric acid, as the resulting oxide layer was then much smoother. When such cathodes were used in a spark gap, groups of low statistical time lags were observed; this supports the view that the oxide layer itself can emit electrons in the gap under the electric field, due to some property of the oxide.

From this conclusion it is now possible to relate this cathode emission to the mean statistical time lag, and in this way to make an estimate of the order of magnitude of the ionization. For, following von Laue (1925) and Zuber (1925) let p_1 be the probability that an electron produced at the cathode leads to spark breakdown; p_2dt the number of electrons produced at the cathode in the time interval dt; dn the number of spark lags which fall within the interval dt at the end of time t; n the number of lags of length greater than t; and N the total number of lags observed. Then

$$n/N = \exp\left\{-\int_0^t p_1 p_2\, dt\right\}.$$

The factor p_1 is a function of the electric intensity, gap distances, and gas density, which, under these conditions, also reduces to a simpler expression dependent on the value of $p_2 \exp(\alpha d)$, where α is the first Townsend coefficient and d the gap distance. If the gap voltage were maintained constant, p_1 would also be constant, so that the mean time lag, T, would then be inversely proportional to the cathode emission p_2, being equal to $1/p_1 p_2$.

Another method of recording the experimental results is given in Figure 5, where $\log n/N$ is plotted against time. If the product $p_1 p_2$ were independent of the time, the above expression for n/N shows that the $\log n/N$ – time curve should be linear. In the present experiments p_1 increased with t owing to the rise of over-voltage with time, so that the relationship should not then be linear, and this is shown by the curves in Figure 5. However, the sharp departure from non-linearity in curve A is in part due to the enhanced electron emission from the oxidized cathode. The reduction in the mean time lag from about 10^{-4} sec. to 56 μsec. and to 20 μsec. must be attributed mainly to the greater cathode emission; and a very approximate estimate of this increase in emission may be made as follows.

When the electrodes were clean and smooth, no sparks were produced within the time interval of the order of 10^{-4} sec., although $V \simeq 2V_s$. Under these conditions p_1 was very high (practically unity). Consequently, the electron emission p_2 must have been very low and probably zero within that interval, giving $n = N$. The reduction of the mean time lag from the value 10^{-4} sec. to, say, 10^{-5} sec. or 10^{-6} sec. must have been due to the cathode emission p_2 attaining high values. When the mean lag T was approximately 10^{-6} sec. the sparking voltage V was about $1{\cdot}03V_s$, and when T was 10^{-4} sec., V was approximately $2V_s$. This reduction of gap voltage to about one-half would have a great effect on p_1, and it is not unreasonable to assume that p_1 would be reduced by a factor of at least 10, owing to the rapid increase of α with V. Hence, since the mean lag was reduced by a factor of 10^2, and p_1 by a factor of 10, the cathode emission must have been increased by a factor of 10^3. Thus it follows that the oxide layer on the tungsten electrodes was able to produce at least a thousand-fold increase in the cathode emission due to the electric field in the gas.

§ 6. MECHANISMS OF CATHODE IONIZATION

Further experiments carried out at high recurrent sparking rates indicated that the mechanism was not thermionic in character, as no effects which could be attributed to any significant accumulation of heat were observed with the active oxidized electrodes. For instance, with spark peak currents of 120 amp. recurring at a rate of 300/sec., the temperature of the whole tube rose only a few degrees. Successive sparks tended to strike at different electrode spots, and oscillograph records showed self-extinguishing of the arc after a few microseconds, and when sufficient over-voltage was applied, two successive spark breakdowns could be obtained at an interval of 10^{-4} sec. with each E.M.F. pulse as shown in Figure 1 (*b*), instead of a prolonged arc. On the other hand, with inactive un-oxidized electrodes each breakdown tended to become an arc, which persisted for the full duration (2 msec.) of the E.M.F. pulse, and which was obviously thermionic. The sparks tended to fix at one electrode hot-spot in the well-known manner for tungsten arcs (Druyvesteyn and Penning 1940), and the electrodes and whole tube rapidly became very hot—a temperature rise of 100 °C. being readily attained with spark recurrent rates of 300/sec. Any increase in over-voltage applied to the gap increased the production of heat by arcing.

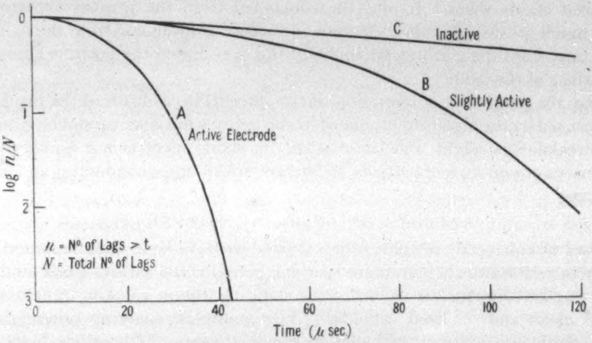

Figure 5. Spark lag distribution.

Enhanced ionization and the resulting steadying of a spark due to the presence of oxides on electrodes has been attributed in some cases, as in the Paetow (1939) effect, to a microscopic discharge produced at an oxide surface and so irradiating the gap independently of its polarity. In the case of a cathode, the positive ions necessary to provide the field could have been produced in the usual pre-breakdown ionization currents in the gas, and on arriving at the cathode have remained on the surface of an insulating oxide film; or they may have been produced as a result of photo-emission from the oxide due to photons from a previous discharge (Druyvesteyn and Penning 1940). Since it took place only from the cathode, it is unlikely that the enhanced electron emission observed from the smooth oxidized tungsten electrodes in a gas was due to the Paetow effect, considered in this sense as a surface discharge phenomenon only, and possible at either electrode. In fact, emission did not appear to depend upon the ionization due to previous spark discharges, although it might well have depended upon the Townsend pre-breakdown current of each spark when the ionization was building up. The emission showed some resemblance to the so-called spray-discharge of Guntherschulze and Fricke (Druyvesteyn and Penning 1940), which was observed with comparatively thick layers (10μ) of an insulating oxide. If the insulating layers were of the order of 10^{-6} cm. thick very high fields could, of course, be produced across them. It must be concluded from the present experiments that a much greater secondary electron emission was produced from the oxidized metal than from the clean metal, and that this was due to the positive charge on the surface of the oxide.

Also, the possibility of ionization due to internal breakdown of the insulating oxide caused by the high field produced by the positive ion layer cannot be ignored: such breakdowns might well occur when the oxide layer is not homogeneous but consists of a mixture of particles of different oxides, some conducting and others insulating.

§7. EFFECTS ON SPARKING POTENTIAL

Cases of enhanced emission from oxidized surfaces have been recorded previously in relation to the minimum sparking potential for various gases, and it is interesting to compare the values of the static minimum sparking potential for various clean and oxidized cathodes. The minimum sparking potentials for nickel, steel, and mercury cathodes in mercury vapour (Llewellyn Jones and Galloway 1938), and for copper, aluminium and steel cathodes in hydrogen (Llewellyn Jones and Henderson 1939), and in deuterium (Llewellyn Jones 1939) have been measured, and the results indicated that the minimum sparking potential for clean surfaces increased with the work function of the cathode. This result is explicable if the coefficient of electron emission from a clean cathode diminished as the work function increased, which is in accordance with emission mechanisms such as those due to the release of kinetic or potential energy of the impinging positive ion (Oliphant and Moon 1931) or to the photoelectric effect of photons from the current. Other hypotheses which regard the emission as thermionic and due to local heating under the impact of positive ions (Kapitza 1923, Sommermeyer 1936) also involve the reduction of γ and, therefore, of sparking potential, with increase of work function.

Normally an insulating oxide film behaves as a negative layer repelling electrons back into the metal and so reducing the emission: but experiment showed that, in all cases measured, oxidation of the cathode lowered the minimum sparking potential, a result which indicated enhanced electron emission from the oxidized surface. Further, it is significant that the effect was noticed both at the minimum sparking potential, when the positive ions were mainly responsible for the electron emission, and at high pressures, when photoelectric effects were important.

The anomalous position of nickel (Llewellyn Jones and Henderson 1939), which gave a minimum sparking potential lower than that expected from the accepted value of the work function for the clean metal, is probably explained by the presence of an oxide film. This is supported by the fact that nickel electrodes have always given comparatively low statistical time lags (Debenham and Haydon 1936, Cobine and Easton 1943); this may be due to the fact that the nickel readily acquired a thin stable oxide layer.*

Thus, both in the previous experiments on the minimum static sparking potential at low pressures and in the present experiments on impulse breakdown at high pressures, enhanced secondary emission was observed from smooth oxidized cathodes, and the results indicate that this is caused by the acquisition of a positive ion layer on the surface of the oxide. This result does not support the hypothesis that the mechanism of emission is thermal in origin, and that the boiling point has an important influence of secondary emission from the cathode (and, therefore, on the sparking potential), as considered by Grigorovici (1939).

§ 8. EFFECTS IN GEIGER COUNTERS

Enhanced electron emission from oxidized cathodes would have important effects in corona discharges from a wire to a coaxial cylinder, especially if the wire were the cathode: oxide layers should facilitate breakdown on the lines indicated above. In Geiger counters, enhanced electron emission from oxide layers would lead to unsteadiness at potentials lower than those corresponding to the breakdown potential for clean electrodes at which counters are operated. Thus when it is necessary to avoid all tendency towards self-triggering it is advisable to maintain the electrodes clean and smooth and as free from oxides as possible. With clean and smooth electrodes and a gap of small volume the present results show that the time lag was approximately 10^{-4} sec., but in counters which have oxidized electrodes the resulting enhanced emission would be likely to produce spurious counts at intervals less than 10^{-4} sec., in spite of the reduced tube potential, because of the greatly increased ionization produced by the oxide. In assessing the relative importance of photo-ionization and the effects of positive ions in the counter discharge mechanism it is necessary to take into account these effects of oxide on the electrodes.

§ 9. CONCLUSIONS

1. Although rough oxidized electrodes lower the spark lag, especially at high pressures, whether as anode or cathode, smooth oxide layers can produce enhanced cathode emission in a gas under an electric field.

2. An oxide layer can thus obscure the influence of the work function of the clean cathode on the sparking potential; oxide layers tend to lower the sparking potential, and also to produce spurious counts in Gieger counters.

3. The mechanism of the enhanced emission is due to the positive charging of the oxide surface, and the results do not support a thermal theory of the emission mechanism.

4. Tungsten electrodes, previously heavily sparked in air and in nitrogen, were found able to produce a pre-breakdown corona glow, which appeared to be

---

* *Note added January* 1949. Recent work (Ivey, H. F., 1948, *Phys. Rev.*, **74**, 983; Wohlfarth, E. P., *ibid.*, 984) indicates that the supposedly anomalous thermionic behaviour of the metals nickel, platinum and zirconium is probably due to surface contamination which is very difficult to remove.

due not only to severe roughening (from oxidation or erosion) but also to minute spike-like growths on the electrodes produced by the sparking. The effect probably illustrates the mechanism by which roughening an electrode ionizes the gap independently of the polarity of the electrode.

ACKNOWLEDGMENTS

The author wishes to thank the Ministry of Supply (Air) for permission to publish this paper, and to express his gratitude to former colleagues at the Royal Aircraft Establishment, Farnborough, for their co-operation and assistance with the oscillographs and the micro-photography. The photographs 1 (*a*), 1 (*b*), 3 (*a*) and 3 (*b*) are reproduced by permission of the Controller of H.M. Stationery Office.

REFERENCES

COBINE, J. D., and EASTON, E. C., 1943, *J. Appl. Phys.*, **14**, 321.
DEBENHAM, W. R., and HAYDON, F. G., 1936, *A.R.C. Tech. Comm., R. and M.* 1744.
DRUYVESTEYN, M. J., and PENNING, F. M., 1940, *Rev. Mod. Phys.*, **12**, 117 (pp. 117–118, 139–140 and 152–155).
GRIGOROVICI, R., 1939, *Z. Phys.*, **111**, 596.
HOWELL, A. H., 1939, *Elect. Engng.*, **58**, 193.
KAPITZA, P., 1923, *Phil. Mag.*, **45**, 989.
VON LAUE, M., 1925, *Ann. Phys. Lpz.*, **76**, 261.
LLEWELLYN JONES, F., 1939, *Phil. Mag.*, **28**, 328; 1945, *J. Soc. Chem. Ind.*, **64**, 317; 1946, *Nature, Lond.*, **157**, 371.
LLEWELLYN JONES, F., and GALLOWAY, W. R., 1938, *Proc. Phys. Soc.*, **50**, 207.
LLEWELLYN JONES, F., and HENDERSON, J. P., 1939, *Phil. Mag.*, **28**, 185.
LOEB, L. B., 1939, *Fundamental Processes in Electrical Discharges in Gases* (London: Chapman and Hall), pp. 497–498.
LOEB, L. B., and MEEK, J. M., 1946, *The Mechanism of the Electric Spark* (Stanford University Press).
OLIPHANT, M. L. E., and MOON, P. B., 1931, *Proc. Roy. Soc.* A, **127**, 388.
PAETOW, H., 1939, *Z. Phys.*, **110**, 770.
ROGOWSKI, W., 1926, *Arch. Electrotech.*, **16**, 496.
SOMMERMEYER, K., 1936, *Ann. Phys. Lpz.*, **25**, 481.
STRIGEL, R., 1925, *Wiss. Veroff. Siemens-Konz.*, **11**, 52.
TESZNER, S., 1946, *Bull. Soc. franç. Electriciens*, **6**, 1.
THOMSON, J. J., and THOMSON, G. P., 1933, *Conduction of Electricity through Gases* (Cambridge: University Press), vol. II, chap. IX.
TILLES, A., 1934, *Phys. Rev.*, **46**, 1015.
ZUBER, K., 1925, *Ann. Phys., Lpz.*, **71**, 25; **76**, 231.

Magnetic Dispersion at Microwave Frequencies

By G. F. HODSMAN*, G. EICHHOLZ† and R. MILLERSHIP
Physics Department, University of Leeds

Communicated by R. Whiddington; *MS. received 25th November* 1948

ABSTRACT. A method is described which has been developed for the measurement of initial permeabilities of ferromagnetic wires in the microwave region and successfully applied over the range from 3 to 13 cm. wavelength to a variety of materials. The measurements are carried out by comparing the attenuations of coaxial transmission lines with the ferromagnetic specimen and with a non-ferromagnetic reference material as inner conductors. The attenuation constants are derived from observations on the input impedance of the line for different terminations as embodied in a circle diagram of impedance. The results are interpreted in the light of modern theories of magnetic dispersion and an estimate of domain sizes is made. The limitations of the theoretical treatments are indicated.

§ 1. INTRODUCTION

Measurements of the variation of magnetic permeability with frequency have been made by a number of investigators. The results are of importance in connection with theories of the domain structure of ferromagnetic materials and with the application of ferromagnetic materials to radio problems. Most of the measurements have been reviewed critically by Allanson (1945), who drew attention to the discrepancy between data published by different authors and to the extreme scarcity of data of any kind at frequencies above 1,000 Mc/s. Inspection of the results published so far seems to indicate that in general no marked variation in permeability has been observed at frequencies below 100 Mc/s., although the wide variations in composition and heat treatment of the materials used by different experimenters renders interpretation of the results difficult. Very few investigators have worked with frequencies above 100 Mc/s., and above 2,000 Mc/s. there were no previous data, with the notable exception of those of Arkadiew (1919) who obtained some results at 2,910, 12,970 and 22,900 Mc/s. The present work was undertaken mainly to remedy this deficiency, particularly as a treatment of domain effects as formulated by Becker (1938, 1939) indicated that a spectacular decrease in permeability was to be expected in the range of centimetric wavelengths.

The work described in this paper was begun with the aim of contributing to the information available on the process of magnetization and the movement of domain boundaries. These movements are primarily determinative of the rate and extent of change of magnetization in a ferromagnetic substance. The precise mechanism of this process is not yet fully understood, but the sequence of changes must depend largely on the shape, size and arrangement of the domains and so on the past history of the material (cf. Stoner 1934, Bitter 1937). The measurement of the permeability under a variety of particular conditions thus provides

---

* Now with L. Oertling Ltd., London.
† Now at the University of British Columbia, Vancouver, B.C.

information relevant to one of the outstanding problems in the theory of ferromagnetism. The present investigation is concerned mainly with the measurement of the initial permeability in small fields so that all boundary movements are of the reversible type; moreover, spin resonance effects of the kind reported by Griffiths (1946) and Yager and Bozorth (1947) are excluded. The problem is complicated considerably by the presence of the skin effect which restricts all magnetic processes to a thin layer near the surface of the material. For microwaves this results in a skin layer which may be thinner than the mean cross-section of the surface domains, so that any change in permeability can be attributed to a reduced effective field strength (cf. Kittel 1946).

Consideration of the skin effect and its relation to magnetic phenomena in high-frequency fields led to the formulation by Hinze (1934) and Becker (1936) of a theory which distinguished two permeability coefficients, commonly referred to as μ_R and μ_L, which result from measurements of resistance and inductance respectively. Of these two coefficients μ_R is always greater than μ_L, which becomes very small at frequencies above 1,000 Mc/s. (Hoag and Jones 1932, Hoag and Gottlieb 1939).

The method described here was designed to permit measurements over a wide range of frequencies and materials. This requirement ruled out immediately any apparatus suitable for use at a single frequency only. As the experiments were aiming at the elucidation of the domain structure of the materials it was also necessary to rule out methods that required machining the specimen into any particular shape after annealing. Owing to the nature of microwave measurement technique, the specimens had to be capable of easy introduction into some kind of transmission system, and in the method adopted finally this was accomplished by using the specimen as the inner conductor of a coaxial line. A system of this kind can be used over a wide range of frequencies, and measurements have been carried out so far over a wavelength range of 3 to 13 cm. with a single transmission line.

§ 2. SURVEY OF METHODS

The following methods have been used or proposed for the measurement of permeability in this region:

(*a*) Reflection of free or guided waves from a ferromagnetic surface.

(*b*) Measurement of the reduced wavelength on a coaxial line as compared with that in air.

(*c*) Measurement of the *Q*-factor of a cavity containing the ferromagnetic material.

(*d*) Measurement of attenuation along a ferromagnetic coaxial line or waveguide.

Reflection methods had been used by Hagen and Rubens (1903) in their measurements at infra-red frequencies, and by Arkadiew (1914) at microwave frequencies with the ferromagnetic specimens in the form of fine wire gratings. Theoretical investigations into the problem of reflection from plane ferromagnetic surfaces (Eichholz and Hodsman 1946) have shown that both for plane free waves and for waveguides the reflection coefficients of ferromagnetic and non-ferromagnetic metals do not differ sufficiently to permit of direct measurement. Only poor conductors seem to be amenable to investigation by this method, and such measurements on ferromagnetic compounds have been reported by Birks (1946).

The method of deducing the permeability from the wavelength difference of the waves travelling along a ferromagnetic wire and in free space has been used by Glathart (1939) at a frequency of 197 Mc/s. At frequencies above 2,000 Mc/s. this method, which leads to μ_L, requires extremely thin wires (about 0·001 cm. radius) and is unsuitable for applications over a wide frequency range as the wavelength difference decreases very rapidly with increase of frequency.

Measurements involving the *Q*-factor of cavities have proved valuable in determinations of dielectric constants in the microwave region. For ferromagnetic materials, most of which are good conductors, the specimen must conform to the internal shape of the cavity and so must either be in the nature of sputtered or plated films or be machined to shape. For the present purpose this method was therefore not regarded as so convenient as method (*d*).

With regard to the attenuation methods, long lossy waveguides have been used by Maxwell (1947) at 24,000 Mc/s. This method is unsuitable at lower frequencies and requires careful machining of long tubes of the substance under test, a requirement that rules out many high-permeability alloys.

Measurement of the attenuation constant of a coaxial line with a ferromagnetic inner conductor is capable of application over a wide range of frequencies and to almost any kind of material. The specimens must be available in the form of wires, but this permits most iron and nickel alloys to be used. The application of this method is based fundamentally on the expression for the attenuation constant of a coaxial line *

$$\alpha=\frac{9{\cdot}95\times10^{6}\sqrt{f}}{\log b/a}\left(\frac{1}{a}\sqrt{\frac{\mu_a}{\sigma_a}}+\frac{1}{b}\sqrt{\frac{\mu_b}{\sigma_b}}\right)\text{ db/m.,}\qquad\ldots\ldots(1)$$

where *a* and *b* are the radii of the inner and outer conductors respectively, which is derived in most textbooks on the subject (cf. Jackson 1945). If a line of length *l* is used and the attenuation is measured first with an inner conductor of ferromagnetic wire and then with one of non-ferromagnetic wire, then the difference in attenuation is given by

$$\Delta\alpha l=(\alpha_1-\alpha_2)l=\frac{9{\cdot}95\times10^{6}\,l\sqrt{f}}{a\log b/a}\left(\sqrt{\frac{\mu_1}{\sigma_1}}-\sqrt{\frac{1}{\sigma_2}}\right)\text{ db.}\qquad\ldots\ldots(2)$$

In this way the effect of the outer conductor and of any other residual attenuation is eliminated and the unknown permeability can be deduced directly from the comparison of the attenuation constants. As the first factor in equation (2) involves only the dimensions of the line and the frequency, all of which can be determined with considerable accuracy, the final result depends mainly on the conductivity of the specimen which is independent of the frequency and can be measured separately at low frequencies. In view of the simple form of equation (2), little difficulty has been experienced in choosing suitable values of *a*, *b* and *l* for the different frequency ranges.

The attenuation constants are determined from observations of the standing-wave pattern in the line which are transformed into values of input impedance for different terminations and plotted as circle diagrams of impedance (cf. Jackson and Huxley 1944, Essen 1944). This method is fairly rapid, accurate and superior in practice to purely arithmetical methods of evaluation. Most of the measurements have been carried out with samples in the form of 26 s.w.g. wires, a very convenient size as it is thin enough to give rise to appreciable attenuation without calling for excessively long lines and yet thick enough to justify the theoretical assumption that the surface area and radius of curvature are large compared with the skin depth. It is quite easy to handle, and thinner wires have been used only in cases where 26-gauge specimens could not be obtained. The line length has been of the order of 1·5 to 2·2 metres for measurements in the 10 cm. region and 1·4 metres in the 3–7 cm. region.

---

* Further terms in this expression are negligible.

§ 3. DESCRIPTION OF APPARATUS

Figure 1 indicates the grouping of high and low frequency components. The main power pack supplies heater and H.T. voltages to the pulse generator, the wavemeter and the amplifier. The pulses produced by the pulse generator are superposed on the grid or reflector voltage of the oscillator in the klystron power pack. The oscillator valves used so far have been reflex klystrons of various types as they produce adequate power for the type of measurement discussed here, permit experiments over a range of frequencies, and lead to a more compact experimental assembly than magnetrons. The high-frequency pulses travel down a waveguide introduced to control the pulse signals and are then fed into the coaxial line system. The inner conductor of the line is formed by the ferromagnetic specimen or the non-magnetic comparison standard, usually constantan. Point A marks the reference plane at which the input impedance of the line is measured. The terminating impedance of the line is varied by means of a shorting piston at the far end of the line or, if the line is short, by a " reactor " piston in a waveguide coupled across the end of the line by a two-piston transformer.

The pulse generator consists of a multivibrator circuit feeding three stages of amplification and produces square pulses of variable amplitude up to 80 v. and a pulse length of 210–270 μsec. The pulse amplifier is a resistance capacity amplifier with selective negative feedback in the first stages. Its circuit is presented in Figure 2, which shows the step attenuator and the method adopted to couple the second detector and output meter.

The maximum overall gain of the amplifier is 120 db., which can be reduced by the calibrated variable and step attenuators to 60 db., thus permitting direct measurement of standing-wave ratios up to 100 times to a uniform degree of accuracy. The overall frequency response represents a compromise solution between the requirements of pulse shape and reduction in noise level. It shows a maximum at 1,300 c/s. with a bandwidth of 1,800 c/s. and a sharp cut-off at the low-frequency side. As the pulse repetition is 1,100 c/s. this leads to slight differentiation of the output pulse, but as a little distortion of the pulse does not affect the accuracy of the standing-wave measurements, this narrow bandwidth serves mainly to reduce the noise level and so to improve the sensitivity of the apparatus.

The type of termination adopted depends mainly on the frequency and the total line length. If the movement of the terminating piston is large compared with the total line length, the resulting impedance points will not lie on a perfect circle, and it is preferable to couple a waveguide across the end of the line. By this means the effective line length is kept approximately constant and comparison tests have shown that the introduction of the waveguide does not result in any increase in the measured attenuation. The specimen is connected to the inner conductor of the standing-wave indicator by a thin tapered connector with a small

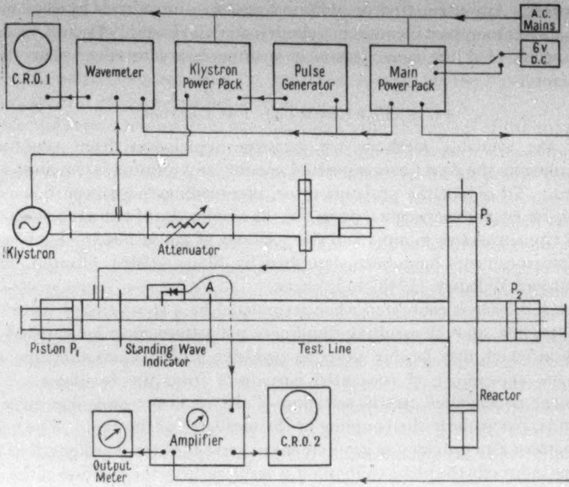
C.R.O. 1
Wavemeter
Klystron Power Pack
Pulse Generator
Main Power Pack
A.C. Mains
6V D.C.
Klystron
Attenuator
P_3
A
P_2
Piston P_1
Standing Wave Indicator
Test Line
Reactor
Output Meter
Amplifier
C.R.O. 2

Figure 1. Layout of apparatus.

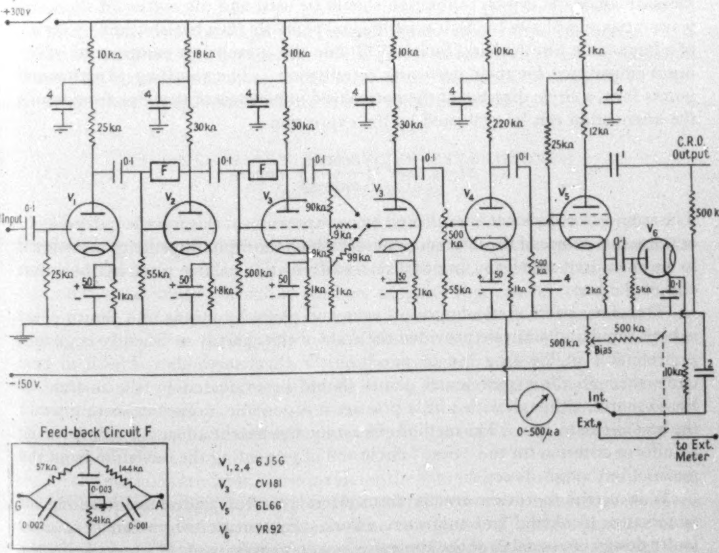
+300V
10kΩ
18kΩ
10kΩ
10kΩ
10kΩ
1kΩ
4
25kΩ
30kΩ
30kΩ
30kΩ
220kΩ
25kΩ
12kΩ
0·1
F
1
C.R.O. Output
Input
V_1
V_2
V_3
V_3
V_4
V_5
V_6
90kΩ
9kΩ
9kΩ
99kΩ
500 kΩ
500kΩ
25kΩ
55kΩ
50
1kΩ
1·8kΩ
55kΩ
500 kΩ
2kΩ
5kΩ
500kΩ
Bias
10kΩ
2
−150V.
0–500μa
Int.
Ext.
to Ext. Meter
Feed-back Circuit F
57kΩ
144kΩ
0·003
G
A
41kΩ
0·002
0·001
$V_{1,2,4}$ 6J5G
V_3 CV181
V_5 6L66
V_6 VR92

Figure 2. Circuit diagram of pulse amplifier.

grub screw. Any attenuation or additional reactance introduced by this connection and its distrene support is common to both materials (Essen 1944) and, by equation (2), cancels. For the same reason it is unnecessary to silver-plate the outer conductor.

§4. EXPERIMENTAL PROCEDURE

Of the available methods for deriving impedances from standing-wave measurements the direct comparison of maxima and minima is the most straightforward. To reduce the probable error, two readings have been taken of each variable for every experimental point, i.e. the amplitudes of two successive maxima and of two successive minima and the positions of the minima. Such standing-wave measurements have been described by Slater (1946), Clayton, Houldin, Lamont and Willshaw (1946) and others.

The indicator is calibrated when terminated by a short-circuit plate in place of the test line, and the resulting standing-wave pattern must be watched for any distortion which may be due either to excessive probe penetration into the line or to the appearance of unwanted harmonics from the oscillator. This requirement necessitates careful selection of the oscillator and alignment of the apparatus, particularly the coupling of the oscillator to the line. The standing-wave pattern also provides an accurate measurement of the wavelength in the line and thus indirectly the phase calibration, a graph relating the position of the minima to the distance in wavelengths from the reference plane. It is often permissible to compute the standing-wave ratios directly, assuming a perfect square law for the crystal detector, particularly if the signal level is high. However, for accurate measurements the crystal calibration should be used and the corrected standing-wave ratios and phases for each experimental point are then transformed by means of a large-scale Smith chart (Smith 1939) into the appropriate components of the input impedance for their particular termination. The resulting experimental points form a circle diagram of the normalized impedance of that line from which the attenuation can be evaluated by the expression

$$\alpha l = \tfrac{1}{2}\cosh^{-1}\left(\frac{\text{centre}}{\text{radius}}\right) \text{ nepers.} \qquad \ldots\ldots(3)$$

The attenuation constant as evaluated by an expression of this form is independent of the actual choice of the reference point at which the input impedance is assumed to be measured or of any impedance transformation taking place at the input end of the line.

Transformation of standing-wave ratio and phase by means of a Smith chart is both rapid and accurate provided the scale of the chart is sufficiently large and is preferable in the long run to purely arithmetical methods. The final best circle through the experimental points should be evaluated by the method of least squares, although with a little practice it is possible in most cases to draw in the best circles by eye. The method of least squares has the advantage of providing a uniform criterion for the "best" circle and of presenting the deviation from the mean of any point directly.

It is useful to review briefly the sources of error under the headings of systematic, accidental and subjective errors. Systematic errors can be due to faulty design or assembly of the apparatus, e.g., eccentricity of the inner conductor or varying penetration of the probe into the line, or to an erroneous assumption in the underlying theory of the method. Most of these errors are self-revealing as they lead to badly distorted circle diagrams or to a distortion of the standing-wave pattern as observed during the crystal calibration. The validity of the assumptions underlying equation (1) has been proved by the "conductivity check" described in the following section.

Accidental errors arising from irregularities in the setting-up of the apparatus, particularly the oscillator, are the most serious cause of errors. Unless the pulse shape observed on the output oscilloscope is maintained for all points along the standing-wave pattern, the measurements are useless, as such pulse distortions are usually due to the presence of some frequency harmonics which result in incorrect readings of both amplitude and phase. Incorrect crystal calibration is shown by a flattening of the resulting circle diagram. Other errors, such as sticking of the probe carriage or bad earthing of the system, will merely lead to an increased scatter of the experimental points in the circle diagram. Similarly all subjective errors show up as irregularities in the circle diagram; erroneous reading or recording displaces a point some distance from the circle and is often self-evident from the sequence of readings. Comparison of results obtained by three different observers over a period of several months has shown that such subjective errors are of little account. It thus appears that all systematic or subjective errors other than those apparent at the beginning of the measurements are either eliminated in the evaluation of the difference of the attenuations or show themselves as increased scatter of the experimental points in the circle diagram. For this reason the probable error decreases with the number of points taken.

The probable error has been evaluated for several typical circle diagrams, and for circle diagrams of 12 to 15 points it has been found that the probable error in the attenuation constant as derived from all the deviations from the best circle is of the order of 0·1 db. irrespective of the actual mean value of αl. Calculation shows that the probable error in the value of the permeability is about 10% for all substances, except nickel, where it is of the order of 15%.

§ 5. SUBSIDIARY AND CHECK EXPERIMENTS

(i) *Initial Permeability*

The high-frequency measurements are significant only if they are related to the low-frequency characteristics of the materials. For this reason particular attention has been paid to the specification of all specimen materials in terms of their D.C. permeability, which is the only property that can be related theoretically to the initial permeability as measured at microwave frequencies. The initial permeability is the limiting value of the ratio B/H for $H \rightarrow 0$. As μ increases very rapidly with field strength for magnetically soft materials, it is important to measure the initial permeability μ_0 at the lowest field strength attainable. Derivation from ballistic determinations of the hysteresis or virgin curves is not very suitable for accurate determinations, and it has been found preferable to use bridge methods.

Of the methods available, those involving the comparison of mutual inductances are the simplest to use, as it is possible to obtain a mutual inductance standard such as the Campbell inductometer. The two forms of bridges that are most easily adapted for these measurements are the Campbell-Heaviside bridge and the Hartshorn bridge (Owen 1946). In the arrangement employed, use has been made of a specially constructed mutual inductance consisting of a long primary coil wound on a 1-in. diameter glass tube and a very short secondary wound on a capillary tube into which the wire specimen can be introduced. With a long wire specimen the demagnetizing effect of this arrangement is negligible. If M_1 and M_2 are the mutual inductances with and without the wire specimen, r and r_1 the radii of the secondary coil and specimen respectively, then the permeability is given by

$$\mu_0 = 1 + (M_1/M_2 - 1)\, r^2/r_1^2. \qquad \ldots\ldots(4)$$

By determining the permeability for different field strengths it is possible to arrive at a fairly accurate value for the constant μ_0. In the present investigation the sensitivity of these measurements has been greatly improved by the use of a 500 c/s. exciting current and the pulse amplifier and output meter instead of a vibration galvanometer.

(ii) *Conductivity Measurements*

As the conductivity is a constant of the material and independent of shape or frequency, it may be measured by one of the usual low-frequency methods. In this particular case measurements have been carried out with the Carey-Foster bridge and the results obtained agree with the usually accepted values for those materials whose characteristics are well defined, e.g. copper, whereas for some of the commercial alloys such as manganin considerable divergencies have been found. A determination of the conductivity of the same materials at microwave frequencies by the use of equation (2) presents a most powerful method of checking both the apparatus and the whole theory underlying these determinations. For two non-magnetic samples equation (2) becomes

$$\alpha l = \frac{9{\cdot}95 \times 10^6\, l \sqrt{f}}{a \log b/a}\left(\frac{1}{\sqrt{\sigma_1}} - \frac{1}{\sqrt{\sigma_2}}\right) \text{db.,} \qquad \ldots\ldots(5)$$

and if one conductivity is assumed to be known, the other one can be derived from the attenuation measurements. Table 1 shows some typical results of this "conductivity check" taken at different frequencies and in different lines.

Table 1. Conductivity Measurements

Material	Conductivity (mhos/metre × 10^6)	
	H.F.	D.C.
Constantan	2·0	1·98
Constantan	1·95	1·98
German silver	4·03	4·10

The agreement between the D.C. value and that derived from the high-frequency measurements is seen to be satisfactory and justifies the following conclusions: (i) equation (2) is fully applicable over the range of centimetric frequencies; (ii) the field strength in the line is small enough for any Hall effect, if present, to be quite negligible; (iii) the conductivity of a material is a constant and independent of frequency, within the frequency range considered. Maxwell (1947) has since published the results of his measurements at a wavelength of 1·25 cm. and arrived essentially at the same conclusion.

(iii) *Other Check Measurements*

Owing to the inherent simplicity of the method it is possible to test independently the effect of changing the parameters of the system. Only the most important ones will be referred to here.

The effective line length l is not very clearly determined by the geometrical dimensions of the line because of the need for a variable termination. If this terminating impedance takes the form of a movable piston at the end of the line, the mean position of the piston may be taken as marking the end of the line, provided the total movement is small. If the terminating impedance is varied by means of the reactor waveguide shown in Figure 1, the length of the line must be determined separately because of the field configuration at the coupling point between coaxial line and waveguide. This has been done by comparing the attenuation of a number of substances for different tube lengths and plotting the resulting values of αl against the apparent tube length l. The point of intersection of the straight lines joining the experimental points for any material indicates the additional length of line due to the termination, as well as the residual attenuation of the coupling.

Checks have been applied to show that the final results are independent of the power level at which the measurements are carried out within the range of the oscillators employed. The power was varied in steps of 10 db.; no difference in αl has been observed. The same result was obtained in experiments with wires of different diameters and for different tube lengths.

The consistency of the measurements has been the subject of a continuous check, as it has been the practice to take at least one set of readings in every run for constantan, which has been the standard reference material throughout; thus standard and specimen are measured under comparable conditions and at that same time a continuous record of experimental conditions had been obtained. Comparison of these constantan circle diagrams has shown that, in general, conditions are very steady and that even the insertion of a number of different specimens in succession does not seriously affect the accuracy of the final results.

§ 6. RESULTS

The following materials have been investigated :

Swedish charcoal iron, white annealed and bright.
50/55 carbon steel, white annealed and bright.
Nickel, commercial, hard drawn.
Mumetal 6, hard drawn.

Of these only the iron and steel wires have been analysed precisely. The iron wire was hard drawn with 90% cold work. The white annealed specimens were annealed with a wet surface at a temperature of 700° c. in an inert atmosphere of burnt town gas (CO, CO_2, N_2), the bright specimens were unannealed. The compositions of the specimens were as follows:

Iron wire: C, 0·03%; Mn, 0·05%; O, 0·002%; Si, P, Cr, Ni, Co, negligible.
Steel wire: C, 0·50–0·55%; Mn, 0·5–0·6%; S, 0·03%; Si, 0·1%; P, 0·02%; Ni, 0·2%; Cr, nil.
Nickel wire: Commercially pure, i.e. Ni$>$99·5%.
Mumetal wire: Ni, 77%; Fe, 15%; Cu, 5%; Cr, 2%; Mn, 0·8%; Si, 0·1%.

The results of the high-frequency permeability measurements, together with the D.C. initial permeability, are given in Table 2.

Table 2. Permeability Results

Frequency (Mc/s.)	Wavelength (cm.)	Iron annealed	Iron bright	Steel annealed	Steel bright	Nickel	Mumetal 6
D.C.	—	180	102	103	65	17	440
2290	13·40	—	74	—	—	—	135
2490	12·40	66	67	48	—	—	—
2830	10·66	61	64	43	60	—	—
3356	—	—	59	—	—	8·3	—
3374	8·89	56	—	41	52	7·5	108
3904	7·68	51	—	37	44	—	—
3956	7·58	—	54	—	—	5·6	98
4260	7·01	—	53	—	—	—	—
4545	6·60	—	52	—	—	5·0	72
4652	6·47	—	—	33	—	—	—
5062	5·93	50	49	32	35	4·1	—
5564	5·39	—	—	31	28	3·4	—
6132	4·89	47	—	30	—	—	—
6432	4·66	—	44	—	25	—	—
6522	4·60	—	—	—	—	3·0	42
8772	3·42	44	36	26	17	1·5	24
9174	3·27	40	33	25	16	—	19
9615	3·12	—	31	23	14	1·03	11
10084	2·97	35	30	22	13	1·0	9

§7. DISCUSSION OF RESULTS

All the materials exhibit a progressive decrease in permeability with increasing frequency. The curves for iron are in general agreement with values obtained by previous investigators, allowing for the use of materials with differing compositions. Arkadiew noted an increase of high-frequency permeability when the material was annealed. This is true of the materials used in this experiment, although it must be pointed out that the D.C. value of the permeability is also higher than for the unannealed specimens. Generally speaking, the frequency at which the decrease in permeability becomes noticeable increases for decreasing values of μ_0.

For the experimental arrangement under consideration it is extremely difficult, if not impossible, to obtain an absolute value of the field strength actually applied to the specimen. Assuming that all the power derived from the oscillator is dissipated in the coaxial line, a value of 0·1 oersted is obtained. This is the upper limit of the field strength, and merely serves to indicate the general order of magnitude of the fields employed.

The initial magnetization of a ferromagnetic may be regarded as taking place in most cases, including all those with which we are concerned, almost entirely by means of reversible shifts of the domain boundaries. The boundary is not a sharply defined surface of separation between the domains but a transition zone in which the individual spins turn gradually and progressively from the direction of magnetization of one domain to that of its neighbour. The application of an external field will cause certain of the spins in this transition zone to become aligned with those in one of the neighbouring domains. This re-alignment of the spins in the boundary region, resulting in the expanding of one domain at the expense of its less favourable orientated neighbour, is equivalent to a movement of the boundary wall as a whole. The speed at which the boundary movements can follow a rapidly alternating field must ultimately depend on the speed at which the spin rotations can be accomplished. As the period of the applied field approaches the relaxation time of the spin rotations, the boundary movements would lag further behind the applied field and the apparent permeability would decrease to unity. For a transverse field there might be a gyroscopic rotation of the spins about internally determined field directions. As far as is known, no rigorous treatment has been carried out for the ferromagnetic case comparable to the treatments for paramagnetic relaxation. Relaxation times in metals have been estimated to be of the order of $10^{-17}-10^{-15}$ sec. The mere assignment of a spin relaxation time cannot therefore account for the ferromagnetic dispersion in the 10^2–10^4 Mc/s. region.

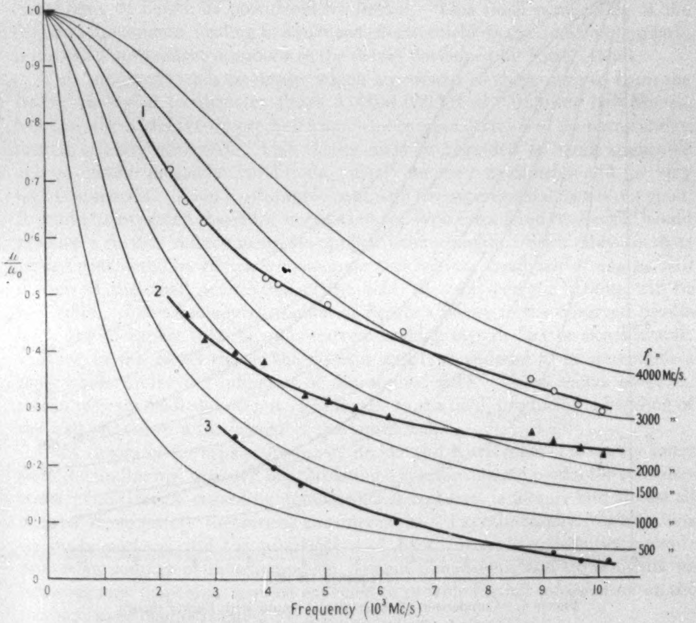

Figure 3. Comparison of experimental curves with Becker theory.
Curve 1: Bright iron. Curve 2: Annealed steel. Curve 3: Mumetal.

A mechanism of retardation of the boundary movement by microscopic eddy currents was first suggested by Arkadiew, and later a theory of ferromagnetic dispersion based on a similar mechanism was developed by Becker (1936). Becker obtains an expression of the form

$$\mu = \frac{\mu_0}{1 + j(f/f_1)}$$

for the permeability μ at a frequency f, μ_0 being the D.C. initial permeability and f_1 a "critical frequency" which, for a simple domain model, may be shown to be dependent upon the domain length and the D.C. characteristics of the material.

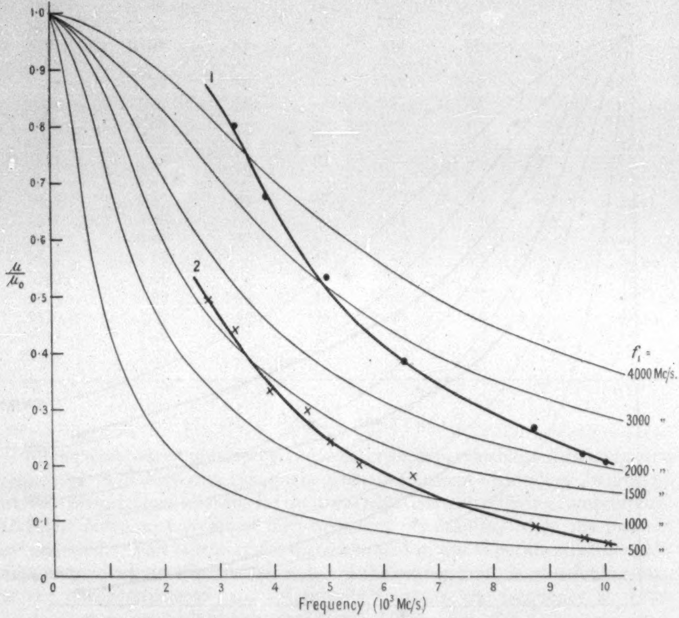

Figure 4. Comparison of experimental results with Becker theory.
Curve 1: Bright steel. Curve 2: Nickel.

Curves derived from this theory for different values of f_1 are given in Figures 3 and 4, together with the experimental curves for the materials investigated. Values of domain lengths, derived from the values of f_1 appropriate to the theoretical curves most approximating to the experimental values, are given in Table 3.

Table 3. Calculated Domain Size

Material	Domain length (cm.)	Material	Domain length (cm.)
Mumetal 6	$1{\cdot}4 \times 10^{-4}$	Iron bright	$9{\cdot}6 \times 10^{-5}$
Iron annealed	$1{\cdot}0 \times 10^{-4}$	Steel bright	$2{\cdot}5 \times 10^{-4}$
Steel annealed	$1{\cdot}6 \times 10^{-4}$	Nickel	$4{\cdot}0 \times 10^{-4}$

The values for domain length given above are not regarded as having any great significance, in view of the discrepancies which exist between the theoretical and experimental curves and the fact that a very simple domain model, namely a cube, is employed for the purpose of calculation. The values obtained are, however, of the correct order of magnitude, if somewhat smaller than the usually accepted values (10^{-3}–10^{-4} cm.).

The theory predicts curves of the same general nature as those obtained for the materials investigated, but appears to require modification in view of the discrepancies which exist in detail. Since the domain length is greater than the skin depth of penetration, the force acting on the domain boundary is not constant throughout its length as postulated by Becker. This small penetration of the field into the domain, leading to a reduced effective field on the domain boundary, is the basic mechanism proposed in the theory developed by Kittel (1946).

This treatment leads to results which are similar to those derived from the Becker theory at frequencies above 3,000–4,000 Mc/s. At lower frequencies, however, the Kittel theory predicts a much more rapid decrease of the permeability than is actually observed. This theory must be regarded as being applicable only to certain particular conditions, namely for very weak fields and for very high frequencies. Even so, the agreement with the experimental data is not good. It would be expected that eddy currents of the type considered by Becker would produce a further reduction in the applied field strength. Such eddy currents are not considered by Kittel, who assumes that for very small field strengths, and in view of the small penetration of the field, the eddy-current braking will be negligible. The close approximation of Becker's theory to the observed results leads one to expect that the eddy-current braking may in fact be considerable. Further, in the Kittel theory the domain wall is considered to be moving as a rigid whole under the influence of the applied field. There seems to be no reason why the wall should not yield locally to the field, producing a bending of the wall instead of a movement of the entire wall.

Any theory of the type proposed by Becker and Kittel must of necessity suffer from the limitations imposed in postulating a specific domain model for consideration. Information regarding domain shapes and sizes is meagre and almost all derived from purely theoretical considerations. Experimentally, observations on Bitter patterns and the propagation of Barkhausen discontinuities provide promising sources of information on domain dimensions, and experiments on ferromagnetic dispersion may be expected to provide further information on the mechanism of magnetization.

The Becker theory, although untenable in its present form in the microwave region, due to the reduced skin depth, does produce an expression with arbitrary constants closely approximating to the experimental results. The postulation of any "frictional force" proportional to the velocity of the domain boundary will reproduce a similar expression, and an attempt has been made, unsuccessfully so far, by Snoek (1945) to explain the "frictional force" in terms of spin–spin interaction. A more detailed discussion of the results from the theoretical aspect will be given in a later paper.

ACKNOWLEDGMENTS

It is a pleasure to acknowledge our thanks to Professor R. Whiddington, under whose general supervision this work has been undertaken, and to Professor

E. C. Stoner for many stimulating discussions. We are greatly indebted to the Captain Superintendent, Admiralty Signal Establishment, for the generous loan of equipment, and to the Superintendent of the Services Electronic Research Laboratory and members of his staff for their help and advice in our oscillator difficulties. We are grateful to the authorities of Leeds University and the Ministry of Education, and one of us (G.F.H.) to York City Council for their financial assistance.

REFERENCES

ALLANSON, J., 1945, *J. Instn. Elect. Engrs.*, **92,** Pt. III, 247.

ARKADIEW, W., 1914, *Ann. Phys., Lpz.*, **45,** 133; 1919, *Ibid.*, **58,** 105.

BECKER, R., 1936, *Ann. Phys., Lpz.*, **27,** 123; 1938, *Z. Tech. Phys.*, **19,** 542; 1939, *Ann. Phys., Lpz.*, **36,** 340.

BIRKS, J. B., *Nature, Lond.*, **158,** 671.

BITTER, F., 1937, *Introduction to Ferromagnetism* (New York and London : McGraw-Hill).

CLAYTON, R. J., HOULDIN, J. E., LAMONT, H. R. L., and WILLSHAW, W. E., 1946, *J. Instn. Elect. Engrs.*, **93,** Pt. III, 97.

EICHHOLZ, G., and HODSMAN, G. F., 1946, *Proc. Leeds Phil. Lit. Soc.*, **4,** 303.

ESSEN, L., 1944, *J. Instn. Elect. Engrs.*, **91,** Pt. III, 84.

GLATHART, J. L., 1939, *Phys. Rev.*, **55,** 833.

GRIFFITHS, J. H., 1946, *Nature, Lond.*, **158,** 670.

HAGEN, E., and RUBENS, H., 1903, *Ann. Phys., Lpz.*, **11,** 873.

HINZE, E., 1934, *Ann. Phys., Lpz.*, **19,** 143.

HOAG, J. B., and GOTTLIEB, N., 1939, *Phys. Rev.*, **55,** 410.

HOAG, J. B., and JONES, H., 1932, *Phys. Rev.*, **42,** 571.

JACKSON, W., 1945, *High Frequency Transmission Lines* (London : Methuen).

JACKSON, W., and HUXLEY, L. G. H., 1944, *J. Instn. Elect. Engrs.*, **91,** Pt. III, 10.

KITTEL, C., 1946, *Phys. Rev.*, **70,** 281.

MAXWELL, E., 1947, *J. Appl. Phys.*, **18,** 629.

OWEN, D., 1946, *Alternating Current Measurements*, 2nd ed. (London : Methuen).

SLATER, J. C., 1946, *Rev. Mod. Phys.*, **18,** 441.

SMITH, P. H., 1939, *Electronics*, **12,** 29.

SNOEK, J. L., 1945, *Monographs on Progress of Reseach in Holland*, No. 19.

STONER, E. C., 1934, *Magnetism and Matter* (London : Methuen).

YAGER, W. A., and BOZORTH, R. M., 1947, *Phys. Rev.*, **72,** 80.

The Measurement of the Specific Heats of some Organic Liquids using the Cooling Method *

BY J. W. LEECH
Queen Mary College, University of London

Communicated by H. R. Robinson; MS. received 16th November 1948

ABSTRACT. The cooling method for the determination of the specific heats of liquids is further developed. The power law of cooling, $d\theta/dt = k\theta^n$, is shown to hold only approximately, and a new method for deducing values of $d\theta/dt$ is described. The specific heats of a number of liquid carbinols are measured over the approximate range 40–70° C.

§ 1. INTRODUCTION

THIS is an account of a continuation of previous work (Ferguson and Miller 1933, Ferguson and Cockett 1940) on the measurement of specific heats of liquids. The method is a refinement of the cooling method in which a small quantity of liquid is contained in a calorimeter placed in a constant temperature enclosure. Measurements are made (*a*) of the rate of cooling $d\theta/dt$ of the calorimeter corresponding to a given temperature difference θ between calorimeter and enclosure, and (*b*) of the electrical power P required to maintain this temperature difference at constant value. To a first approximation these quantities are related by the equation $P = Wd\theta/dt$, where W is the heat capacity of the calorimeter and contents.

---

* The paper forms part of a Thesis submitted for the Ph.D. degree of the University of London.

Values of W relate to specific values of T, the absolute temperature of the calorimeter system; from them may be deduced the corresponding values of S, the specific heat of the liquid in the calorimeter, since $W = W_c + mS$, where W_c is the heat capacity of the calorimeter alone, determined in a preliminary calibrating experiment using a liquid of known specific heat, and m is the mass of liquid in the calorimeter.

§ 2. APPARATUS

The apparatus was essentially that used by Ferguson and Cockett, and only details of difference will be described. The calorimeter and enclosure are shown diagrammatically in Figure 1.

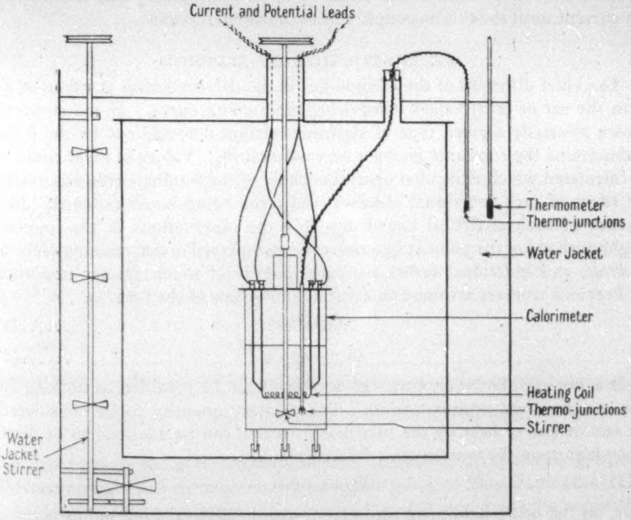

Figure 1. Diagram of apparatus.

The heating coil was again of constantan, but its resistance was increased to approximately 5 ohms in order to reduce the magnitude of the maximum heating current required. Both coil and thermocouple were coated with a thermosetting varnish (Damarda lacquer L3126*); two layers of varnish gave adequate insulation and, judging from the lack of discoloration, were completely unaffected by any of the liquids investigated.

---

* Kindly supplied by Messrs. Bakelite Ltd.

The thermocouple consisted of five junctions in series instead of three, and by a change of galvanometer the unbalance sensitivity when reading its E.M.F. was increased to about 2 mm/μV.

§ 3. EXPERIMENTAL PROCEDURE

The experimental procedure fell into two parts: (*a*) the delineation of the complete cooling curve starting with the calorimeter at a temperature some 50° C. above that of the enclosure, and (*b*) the determination of the power required to maintain the temperature difference between calorimeter and enclosure constant at various values.

The cooling curve was traced by heating the calorimeter to a temperature some 60° C. above that of the enclosure, switching off the heating current and then making observations of the thermocouple E.M.F. at intervals, first of 1 minute, and, as the rate of cooling decreased, lengthening to 4 or 6 minutes.

The power observations were straightforward. Since the heating coil resistance remained constant to within 1 part in 2,000 over the range of heating currents employed, it sufficed to measure the potential difference across a standard 0·01 ohm resistance in series with the heating coil after first adjusting the current until the thermocouple E.M.F. remained constant.

§ 4. DISCUSSION OF METHOD

The chief difficulty of the method lies in the determination of values of $d\theta/dt$ from the set of (θ, t) values comprising the cooling curve. If the curve were known to satisfy a given type of algebraic relation it would not be too difficult to determine the constants giving a curve of best fit. Values of $d\theta/dt$ could then be calculated which depended upon the whole of the cooling curve observations, the effect of each individual observational error being much reduced. In the absence of such analytical knowledge only the observations in the immediate neighbourhood of the point in question can be employed in determining each value of $d\theta/dt$, and individual errors are consequently of much greater importance.

Previous workers assumed an accurate power law of the form

$$d\theta/dt = k\theta^n \qquad \ldots\ldots(1)$$

or

$$\theta^{1-n} = at + b. \qquad \ldots\ldots(1')$$

It is obvious, however, that such a relation can be regarded as nothing more than a convenient approximation. The primary quantity to be considered is the rate of loss of heat by the calorimeter, which can be assumed to be directly dependent upon the temperature difference θ, i.e.

$$dQ/dt = f(\theta). \qquad \ldots\ldots(2)$$

$d\theta/dt$, on the other hand, is a secondary quantity derived from dQ/dt according to the relation

$$\frac{dQ}{dt} = W\frac{d\theta}{dt}, \qquad \ldots\ldots(3)$$

where W, the heat capacity of the calorimeter system, is itself a function of θ. It would thus require a very special set of circumstances for the relation (1) to hold with any accuracy.

In spite of this argument, the power law assumption does form a very useful approximation. The method of analysis of the cooling curve employed involves the assumption of a convenient value of the index n and the calculation of values of θ^{1-n} corresponding to each value of θ in a given set of cooling curve observations. These values of θ^{1-n} when plotted against the corresponding values of t give curves which are very nearly linear (see Figure 2). It is next assumed that small segments of the curve can be regarded as being accurately linear and the gradient δ of the best straight line through each consecutive group of 10 or 20 points is calculated using the method of averages. Each value of δ so obtained is assumed to represent the gradient of the (θ^{1-n}, t) curve at the centroid of the corresponding group of points, thus:

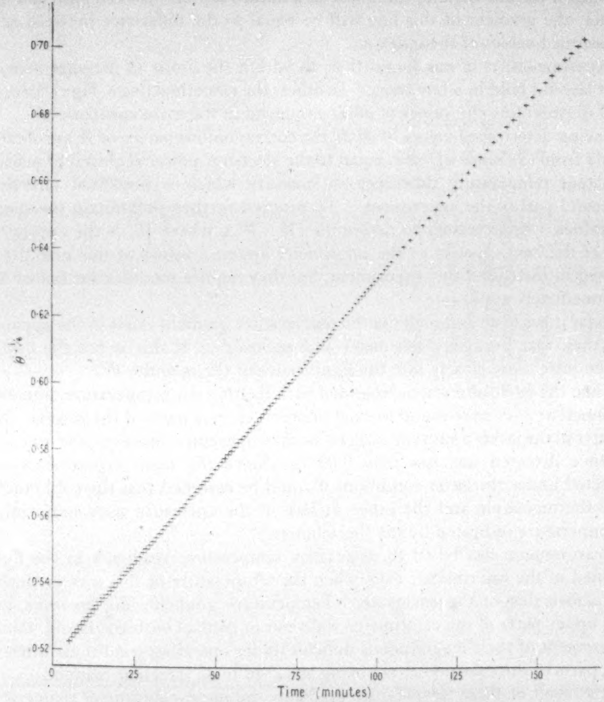

Figure 2. Cooling curve $(\theta^{-\frac{1}{4}}, t)$ for experiment using water.

$$\delta = \frac{d}{dt}(\theta^{1-n}) = (1-n)\theta^{-n}\frac{d\theta}{dt}. \qquad \ldots\ldots(4)$$

A practical test of the validity of the power law relation can now be derived. If the law is valid but the index has a value m, differing from the assumed value n, we have

$$d\theta/dt = k\theta^{m}; \qquad \ldots\ldots(5)$$

thus, combining the relations (4) and (5),

$$\delta = k(1-n)\theta^{m-n}$$

or

$$\log \delta = \log(\text{const.}) + (m-n)\log\theta. \qquad \ldots\ldots(6)$$

Thus, if the law is valid, there will be a linear relation between $\log\delta$ and $\log\theta$. Further, the gradient of this line will be equal to the difference between actual and assumed values of the index n.

Experimentally, it was found that, to within the limits of measurement, the power law did hold in a few cases. In others the smoothed ($\log\delta$, $\log\theta$) curve was useful in providing the values of $d\theta/dt$ employed in the main calculations.

Having determined values of $d\theta/dt$, the corresponding values of W are obtained directly from (3), since dQ/dt is equal to the electrical power required to maintain a constant temperature difference—a quantity which is measured directly in the second part of the experiment. To proceed further, and obtain the specific heat values, it is necessary to determine $(W - W_c)$, where W_c is the appropriate value of the heat capacity of the calorimeter system; values of this quantity are obtained in the calibrating experiment, but they require modification before they are immediately applicable.

So far it has been assumed that no temperature gradient exists in the apparatus other than that between calorimeter and enclosure. If this is not the case we must enquire more closely into the significance of the quantity θ.

When the enclosure was surrounded with melting ice, temperature differences of as much as 2° c. were found to exist between various parts of the jacket. With the water in the jacket approximating to room temperature, however, the maximum difference detected was less than 0·02° c. Since the main experiments were conducted under the latter conditions it could be assumed that the cold junction of the thermocouple and the inner surface of the enclosure were uniformly at the temperature indicated by the thermometer.

Measurement also failed to detect any temperature gradients in the liquid contained in the calorimeter, even when the temperature of this was as much as 50° c. above that of the enclosure. Temperature gradients do, however, exist in the upper parts of the calorimeter walls not in contact with the liquid, though measurement of their magnitude is difficult under operating conditions when the upper parts of the calorimeter are being splashed in an irregular manner.

As a result of these temperature gradients the mean calorimeter temperature θ' is less than that indicated by the thermocouple θ and the difference $(\theta - \theta')$ is greater the less liquid is contained in the calorimeter. The heat capacity of the calorimeter W_c will vary with θ', and it will be seen that, given a fixed value of the absolute temperature of the calorimeter liquid, W_c will vary with the amount of liquid; values of W_c obtained in a calibrating experiment will therefore only apply to other experiments employing the same volume of liquid.

Associated with the decrease in mean calorimeter temperature is a corresponding decrease in the electrical power required to maintain a constant temperature difference. This is shown in Figure 3, which gives curves of $\log C$ (effectively log power) *vs* $\log\theta$ for a number of experiments, for it is seen that the curves are, with one minor exception, in the order of the volumes of liquid employed. These curves may be used to derive small corrections to be applied to the values of W_c obtained in the calibrating experiment.

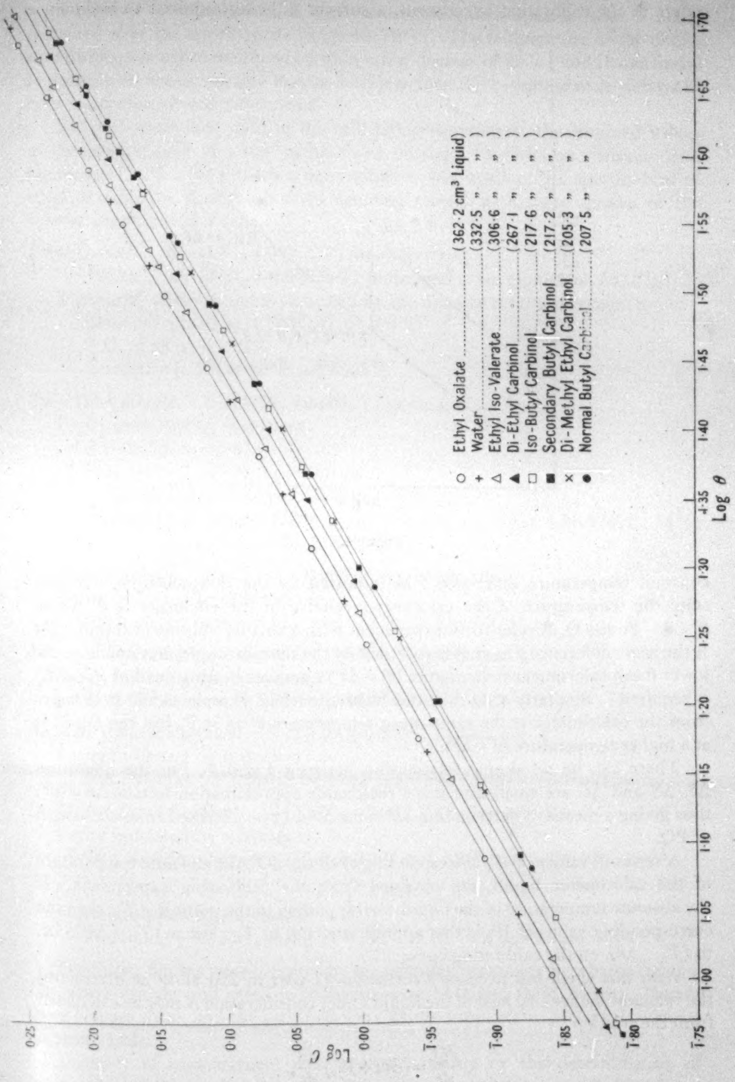

Figure 3. (Log *C*, log *θ*) curves.

Consider portions of two ($\log C$, $\log \theta$) curves as in Figure 4. The point P refers to the calibrating experiment, a current C being required to maintain a

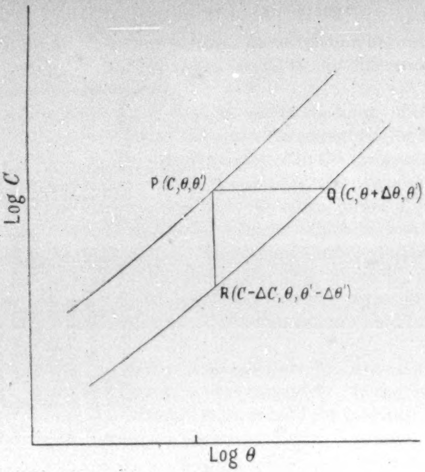

Figure 4.

constant temperature difference θ as indicated by the thermocouple. In this state the temperature of the calorimeter relative to the enclosure is θ' where $\theta' < \theta$. Points Q, R refer to an experiment with a smaller volume of liquid. At R the same difference θ as at P is recorded by the thermocouple, but owing to the lower mean calorimeter temperature $(\theta' - \Delta\theta')$ a smaller heating current $(C - \Delta C)$ is required. Similarly at Q the same heating current C replaces the heat losses from the calorimeter at the same mean temperature θ' as at P, but the liquid is at a higher temperature $(\theta + \Delta\theta)$.

There can be no simple relationship between θ and θ', but the quantities $\Delta\theta$, $\Delta\theta'$ and ΔC are small, and it is a reasonable approximation to take $\Delta\theta = \Delta\theta'$, thus giving a means of determining $\Delta\theta'$ since $\Delta\theta$ may be obtained from the length of PQ.

A series of values of W_c corresponding to those of T, the absolute temperature of the calorimeter liquid, are obtained from the calibrating experiment. If the absolute temperature of the liquid corresponding to the point R is T_R, then the corresponding value of W_c is that appropriate, not to T_R, but to $(T_R - \Delta\theta')$, i.e. to $(T_R - \Delta\theta)$, on the calibrating curve.

With this small but necessary correction (1 part in 250 of W at maximum) the values of the specific heat of the liquid under consideration S may be calculated from the relation

$$\frac{dQ}{dt} = (Sm + W_c)\,\frac{d\theta}{dt},$$

where m is the mass of the liquid.

§ 5. RESULTS OF MEASUREMENTS

A number of organic liquids were investigated, their specific heats S being measured over the approximate range 40–70° c. The temperature of the enclosure during the experiments was within a few degrees of 20° c., and it was found impossible to obtain reliable results with less than 20° c. temperature difference between enclosure and calorimeter.

Distilled water was used in the calibrating experiment, the assumed values of the specific heat of water being those obtained by Osborne, Stimson and Ginnings (1939). As a check a determination was made of the specific heat of ethyl oxalate, the results obtained agreeing closely with those quoted in the *International Critical Tables.*

Ethyl Oxalate. $S=(1{\cdot}81_4+0{\cdot}002_7\,T)$ joules/gm° c.
cf. $(1{\cdot}81_2+0{\cdot}00276\,T)$ joules/gm° c. as quoted in *I.C.T.*).

The purity of the liquid is indicated by the manufacturer's statement:
"Ester calculated as $(COOC_2H_5)=100\%$.
S.G. at 15° c. = 1·085.
Refractive index at 20° c. = 1·4105."

Ethyl Iso-Valerate. $S=(1{\cdot}89_9+0{\cdot}004_5\,T)$ joules/gm° c.
Purity indicated by statement:
"S.G. at 15° c. = 0·873.
Free acid = 3 cm³ N/1. per 100 gm.
Ester calculated as $C_4H_9COOC_2H_5=99{\cdot}5\%$.
Boiling range: below 132° c., 5%; 132–134° c., 33%; 134–136° c., 54%; 136–138° c., 5%."

Iso-Butyl Carbinol. $S=(2{\cdot}20_8+0{\cdot}008_4\,T)$ joules/gm° c.
Purity indicated by statement:
"100% distils between 128° and 132° c. (B.P. = 130·5° c.)."

Normal Butyl Carbinol. $S=(2{\cdot}18_0+0{\cdot}006_3\,T)$ joules/gm° c.
Purity indicated by statement:
"95% distils between 134·5 and 138·5° c. (B.P. = 137·9° c.)."

Secondary Butyl Carbinol. $S=(2{\cdot}36_7+0{\cdot}005_2\,T)$ joules/gm° c.
Purity indicated by statement:
"Not less than 95% distils between 125·0 and 131·0° c. (B.P. = 128° c.)."

Di-Methyl Ethyl Carbinol. $S=(2{\cdot}60_9+0{\cdot}009_3\,T)$ joules/gm° c.
Purity indicated by statement:
"95% distilling between 113·6 and 117·6° c. (B.P. = 115·6° c.)."

Di-Ethyl Carbinol. $S=(2{\cdot}74_4+0{\cdot}004_2\,T)$ joules/gm° c.
Purity indicated by statement:
"Initial B.P. = 99·5° c., final B.P. = 103·0° c. (B.P. of pure liquid = 101·8° c.)."

The purity figures were supplied by the manufacturers as typical batch figures. The ethyl oxalate and ethyl iso-valerate were obtained from Messrs. British Drug Houses, Ltd., and the carbinols were kindly supplied by Messrs. Industrial Solvents, Ltd.

Accuracy of measurement was governed mainly by the determination of $d\theta/dt$ and was estimated at 1 part in 400. To this order it was considered unnecessary to carry out further purification of the liquids.

§6. CONCLUSIONS

As has already been stated, inaccuracies in the determination of $d\theta/dt$ were the chief limitations in the present series of experiments, and there has, therefore, been no discussion of a number of secondary factors which would have to be taken into account if a much higher accuracy was aimed at. Such secondary factors include the state of the surface of the calorimeter and of the enclosure, the absolute temperature of the calorimeter system (in addition to its temperature relative to the enclosure), the rate of stirring of the calorimeter liquid, and the atmospheric pressure. It is considered, however, that the most useful development of the method would be along the lines of obtaining the same accuracy as at present but with simplified procedure rather than of greatly improved accuracy.

Tentative suggestions for simplification are (*a*) the mounting of the calorimeter system so that it can be refilled without dismantling, and (*b*) the incorporation of some inertialess instrument such as a cathode-ray oscilloscope to determine the balance point when measuring thermocouple E.M.F.'s under conditions of cooling. With such improvements it should be possible to make fairly rapid measurements of specific heats of liquids available in quantities of the order of 100–300 cm^3.

§7. ACKNOWLEDGMENTS

Thanks are due to Professor H. R. Robinson for the use of laboratory facilities and for kindly and helpful advice, and to Dr. A. H. Ferguson, who suggested the problem and supervised it in its early stages.

REFERENCES

Ferguson, A. H., and Cockett, A. H., 1940, *Phil. Mag.*, **29**, 185.

Ferguson, A. H., and Miller, J. T., 1933, *Proc. Phys. Soc.*, **45**, 194.

Osborne, N. S., Stimson, H. F., and Ginnings, D. C., 1939, *Bur. Std. J. Res., Wash.*, **23**, 197.

LETTERS TO THE EDITOR

D.C. and Pulsed Emission from Oxide Cathodes

In a recent publication (Wright 1949), the writer has shown that the difference between " pulsed " and D.C. emission from oxide cathodes is due to a decay effect with a time constant which is between 1/1,000 and 1/100 sec. at the higher temperatures, and longer at lower temperatures. This decay causes the steady-state D.C. emission at the higher temperatures to be less than the instantaneous emission which, however, is identical with the pulsed emission. The steady-state emission is between 1/2 and 1/20 of the pulsed emission at 760° C. in the diodes under test, and the ratio varies with temperature. Thus Richardson plots for the two types of emission are not parallel.

Further investigation of these curves with base metals chosen to introduce negligible interface effects, i.e. pure nickel, and nickel with 0·1% Al or 0·2% Ti, has established that they have the typical form shown in curves (*a*) and (*b*) of the Figure. During operation under D.C. conditions at from 1 to 2 amp/cm^2, the pulsed emission remains constant for many hundreds of hours, but the D.C. emission falls continuously, curves (*c*) and (*d*). It is clear now that this is because the decay effect becomes more pronounced, and that the decay is due to " poisoning " of the emission by ions returning from the anode or anode–cathode space to the cathode. If D.C. performance only were observed, these results might be attributed to a real decrease in the emission available from the coating. The present results show, however, that the coating potentiality for emission is unimpaired, since pulsed emission is constant and recovery of D.C. emission in an " off " period is rapid. A similar decrease in emission was recently observed by Metson and Holmes (1949) in the triode portion of their special diode–triode tube, but not in the diode portion. The increased poisoning is almost certainly due to the development of deposits on the anode surface, formed primarily of substances liberated from the cathode. These deposits dissociate under electron bombardment, liberating gas which returns to the cathode as positive ions. The decay effects are found to set in at lower anode voltage and current as the operation continues.

That the difference between D.C. and pulsed emission is due to gas "poisoning" has been shown by tests using various special diodes, in which it has been possible to observe equal D.C. and pulsed emissions at the higher temperatures for short periods, for example after bombarding a tantalum anode to 1,200° C., or after bombarding off the visible film from a nickel anode at 800° C., so causing ionization of barium vapour. The D.C. and pulsed emissions have remained equal for longer periods in a diode with two anodes, one facing the cathode and the other alongside it, so that electrons could be deflected to the latter with a magnet, after normal activation using the first anode. The D.C. emission to the second anode was equal to the pulsed emission to either.

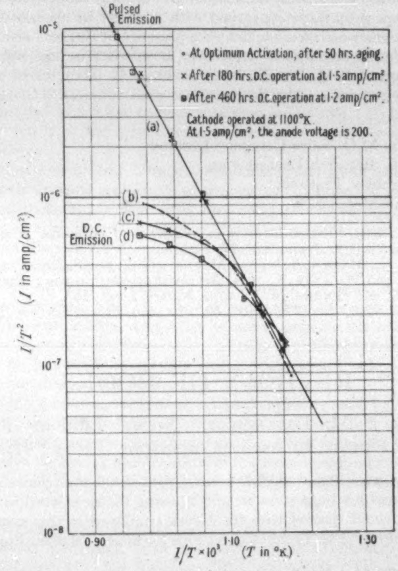

Richardson plot according to the equation $I = AT^2 \exp(-\phi/kT)$.

The Figure shows that the D.C. plots are not linear, presumably because the state of the surface varies with temperature. At the higher temperatures the higher emission produces a larger ion current which causes increasing modification of the surface, probably by removing surface barium, though this is not the only possibility. In such a case the D.C. work function as obtained from experimental Richardson plots would have no true physical significance, nor would the fact that its apparent value is lower than the pulsed work function. The corollary is that the pulsed emission arises from a surface fully covered with barium, and the D.C. emission at the higher temperatures comes from a surface almost completely denuded of barium by ion bombardment. The work function for pulsed emission is 1·6 ev. in the Figure, and the associated A value in the Richardson equation is 100. Work functions of this order have been obtained in many of our recent measurements, and, moreover, have varied only slightly during various activating and de-activating treatments, which have caused considerable variations in apparent D.C. work function and wide variations in the activation energy for conductivity, which was measured at the same time. These results are not consistent with a simple semiconductor model, but rather support the view that the pulsed emission is derived by thermal ionization of the adsorbed barium, as in de Boer's theory (1935). This will remain possible as long as surface barium is present, i.e. in pulsed operation, in D.C. emission tests at low temperature where the dissipation is low, and in D.C. operation with anode voltage too low to cause ionization (Metson and Holmes 1949).

One cannot deduce with certainty the properties of the " clean " surface of the activated coating, but it is an interesting possibility that the work function may be near 1·0 ev., i.e. lower than the pulsed work function. The low emission of the clean surface would then be due to the low *A* value, due in turn to the high expansion coefficient (Eisenstein 1946, Wright 1949). If this is so, many difficulties in forming models for the oxide coating would disappear, especially those concerned with presence or absence of surface barium, since many observations which seem to deny the presence of surface barium have been made under ion bombardment conditions. Moreover, if this is true, the semiconductor model (Hermann and Wagener 1944, Wright 1949) could apply to the clean surface case, since this model seems to require a rather low external work function (Hermann and Wagener 1944, Wright 1948).

Research Staff of the M.O. Valve Company Limited
at the G.E.C. Research Laboratories,
Wembley, England.
24th March 1949.
D. A. WRIGHT.

DE BOER, J. H., 1935, *Electron Emission and Adsorption Phenomena.* Cambridge.
EISENSTEIN, A., 1946, *J. Appl. Phys.*, **17,** 434.
FRIEDENSTEIN, H., MARTIN, S. L., and MUNDAY, G. L., 1948, *Rep. Prog. Phys.*, **11,** 298.
HERMANN, G., and WAGENER, S., 1944, *Die Oxydcathode* (Leipzig : Barth).
METSON, G. H., and HOLMES, M. F., 1949, *Nature, Lond.*, **163,** 61.
WRIGHT, D. A., 1948, *Proc. Phys. Soc.*, **60,** 23; 1949, *Proc. Phys. Soc.* B, **62,** 188.

REVIEWS OF BOOKS

Micromeritics, by J. M. DALLAVALLE. Second Edition. Pp. xxviii+555. (New York : Pitman Publishing Corporation, 1948). 42*s.* 6*d.*

The author suggests a new word, *Micromeritics*, to mean the science and technology of fine particles, and gives his suggestion weight by using the new word as the title of a very fine book. No one could quarrel with the Greek employed in this synthesis but, on the other hand, the sub-title, "The Technology of Fine Particles", is plain English and describes the book exactly.

Expensive scientific books are not usually set out to catch the eye. This one, like other books from the same publishers, is different. The bright red, white and black dust cover and the cream boards will inevitably stimulate curiosity in a laboratory or scientific library. The agreeable appearance is backed up by excellent paper, printing and diagrams. Perhaps partly in fun, but none the less with sound business judgment, the printers and publishers have subjected the scientists to the powers of modern advertising, and they have done this with good taste. The book is as smart as a new chromium desk lamp.

As for the contents of the book, they resemble an encyclopaedia. The twenty-three chapters are distinct and each covers a wide field. Broadly speaking, the arrangement is as follows. First comes the dynamics of a single particle in a viscous medium, including applications such as the centrifuge. The next seven chapters deal with the shapes of particles, distribution functions, the methods of particle size measurement, the theory of sieving and grading, packing, voids and the behaviour of aggregates under pressure, diffusion of particles and the electrical and sonic properties of particles in a carrying fluid. The following six chapters describe the heat conductivity of packings, the relationships between surface energy, heats of wetting and the like, special aspects of the physical chemistry and chemistry of small particles such as crystal growth and oxidation, the flow of fluids through packings, particle-moisture relationships and capillarity. Chapter 16 describes methods of measuring particle surface. Chapter 17 is about muds and slurries. Chapter 18 summarizes work on the transport of silt in rivers and of muds and slurries through pipes and nozzles. The following three chapters are about dust storms, dust in the atmosphere and industrial dust, and the methods of separating dust from air. Chapter 22 is a short account of fine grinding. The last chapter discusses the application of statistics to sampling as well as giving a critical commentary on the experimental procedure. Finally, there is a bibliography containing a list of over 400 papers, seven appendices, an author index and a subject index.

The author has spared no pains to make the book comprehensive and quickly usable. The list of contents gives chapter headings and paragraph headings. There is a four page list of the principal symbols and the dimensions of the quantity symbolized. The indexes are excellent, and the bibliography quotes all titles in full in their original language (sometimes with a translation) and the exact reference details. Each chapter is concluded with about half a dozen problems. Some are merely numerical substitutions in formulae given in the text; others are more general and do illustrate and amplify the text. The reader is also helped, where necessary, by the inclusion of sections summarizing fundamental ideas lying at the fringe of the main subject. For example, ten pages are given to the theory of diffusion by turbulence; several pages are given to the various corrections to Stokes' law; and the theory of the coagulation of smokes receives a section on its own. Enough is said to make clear to the reader that if he has a special interest in these matters, a study of the original literature is unavoidable.

The book contains a very large number of equations, and about twenty per chapter are considered sufficiently important to justify a number. Sometimes the equations are derived from commonly known laws, but frequently they are quoted from original papers as representing the best fit to experimental results. The more academic reader might feel a little uneasy at finding on the one hand equations with a sound fundamental basis, such as the Rayleigh scattering formula, and on the other hand empirical equations, such as Gilbert's, for the amount of silt moved by a stream. The scope of the book, however, unavoidably reaches into regions of science where progress depends more on experiment than on abstract contemplation. The author often does what he can to indicate the reliability and range of the empirical formulae, and sometimes makes a short but valuable criticism. The monumental effort that he has made in reading and summarizing a voluminous and scattered literature deserves our thanks and praise.

The book is highly recommended for all scientific libraries used by chemists, physicists, mathematicians and civil engineers. Physiologists also will find sections of the book informative. Industrial research laboratories encountering problems of dust hazards will probably already have the works and technical side covered comprehensively, and the value of the book to them will lie in its description of scientific fundamentals. W. G. P.

Modern Operational Calculus, with Applications in Technical Mathematics, by N. W. McLachlan. 1st Edition. Pp. xiv+218. (London: Macmillan, 1948). 21*s*.

Those to whom the technical applications of mathematics are of importance are still further indebted to Dr. McLachlan by the appearance of this book. It is described as " addressed to the technical reader whose mathematical training covers a more restricted field than that of the pure mathematician ". With this in mind quite extensive appendices are provided—in length about one-quarter of that of the text. They cover subjects such as Heaviside's unit function, the convergence of infinite series and integrals, together with brief notes on special topics, e.g. the Mellin inversion theorem. The difficulties of the student who is at such a stage that he meets for the first time the theory of (say) infinite integrals will be considerable, but a patient and careful application should surmount them, and prove itself well spent.

The Laplace transform $\phi(p)$ of a function $f(t)$ is defined here in its operational form, viz. :

$$\phi(p)=p\int_0^a e^{-pt}f(t)\,dt.$$

This relationship is written symbolically as $f(t) \supset \phi(p)$, $\supset$ being a U lying on its side. The closed end always points to the transform. Chapter I gives this definition, and discusses briefly questions of discontinuity, boundedness, continuity and convergence.

Chapter II establishes theorems or rules expressing the Laplace transforms of functions of $f(t)$ in terms of $\phi(p)$, the transform of $f(t)$ itself. It is these results that constitute the basis of the application of the method to the solution of so many problems.

Later chapters deal with the solution of ordinary linear, and partial linear, differential equations and the evaluation of integrals. The parts dealing with differential equations are freely illustrated by examples drawn, in the main, from the theory of transmission lines and electrical networks.

The last two chapters deal respectively with the derivation of Laplace transforms of a number of functions, and the application of the transform method to problems of impulses. This last topic is dealt with very fully, and will be a main centre of interest to many readers.

The production of the book is very commendable. One misprint, on page 205, was the only one noted in the course of reading it, and this error, viz. " Fouriere xpansions ", will cause more smiles than confusion. H. H. HOPKINS.

The Measurement of Stress and Strain in Solids. Pp. xii + 114. (" Physics in Industry " Series; Institute of Physics, London, 1948.) 17*s.* 6*d.*

The stresses and strains in a bridge or a steam engine can be calculated from a few elementary formulae ; the calculation of the stresses in the root of a turbine blade, or in a fast aircraft subjected to vibrations, is however, too difficult to be a practical proposition. In such cases, methods of measuring static or cyclic stresses on models or under working conditions have to replace calculations based on the theory of elasticity.

A number of such experimental methods of stress measurements have been developed during the last twenty-five years; some of them, like the photoelastic and the electric wire resistance gauge methods, have become engineering tools of the highest importance. Owing to the recent origin of this development, many engineers and physicists are not aware of the availability of instruments that could be used in their work to great advantage, and the present volume fulfils a valuable mission by addressing the potential users of the new methods.

Like the other booklets of the series " Physics in Industry ", it does not claim to be as complete and balanced as a work written for specialists; its obvious purpose is to make its readers aware of new developments, rather than to give them a working knowledge. It is based on a conference held by the Manchester and District Branch of the Institute of Physics in 1946, and contains contributions from eleven authors covering a large number of methods of measurement of stress and strain in solids.

It begins with an excellent account of the physical characteristics of wire resistance gauges by the late Mr. E. Jones; the use of such gauges for determining complex states of stress is discussed by Dr. F. Aughtie. Mr. W. A. P. Fisher gives a brief but valuable review of recent developments in photoelasticity; and Dr. G. E. Bennett discusses electromagnetic and electrostatic stress indicators. Mr. D. E. Thomas describes his own technique of strain measurement by x rays; his contribution would have gained by taking into account other (in some respects more orthodox) x-ray methods, at least in the form of references. Brief notes have been contributed by Dr. E. P. George, Mr. F. B. Bull, Mr. H. McG. Ross, Mr. J. W. Fitchie, Mr. C. E. Phillips and Mr. K. J. Pascoe. E. OROWAN.

CORRIGENDUM

Review of " Vision and the Eye ", by M. H. PIRENNE (*Proc. Phys. Soc.* B, 1949, **62,** 338).

Line 21 of this review, *for* " .... of a photoreactive field " *read* " .... of a photometric field ".

CONTENTS FOR SECTION A

PAGE

Mr. T. K. Jones, Dr. R. A. Scott and Dr. R. W. Sillars. The Structure and Electrical Properties of Surfaces of Semiconductors.—Part I. SiC . 333

Dr. A. J. Elleman and Dr. H. Wilman. The Structure and Epitaxy of Lead Chloride Deposits Formed from Lead Sulphide and Sodium Chloride . . 344

Dr. E. W. Kellermann and Mr. K. Westerman. On the Absorption Spectrum of Cosmic Rays 356

Dr. S. M. Mitra and Mr. W. G. V. Rosser. Momentum Spectrum of the Particles in Extensive Air Showers 364

Dr. H. Elliot. The Effect of External Quenching on the Life of Argon–Alcohol Counters 369

Prof. W. Heitler and Prof. L. Jánossy. On the Absorption of Meson-producing Nucleons. 374

Dr. J. Rzewuski. Some Cut-off Methods for the Electron Self-Energy . . 386

Letters to the Editor :

Mr. R. P. Hudson, Miss B. Hunt and Dr. N. Kurti. The Use of Liquid Helium in Magnetic Cooling Experiments 392

Prof. E. N. da C. Andrade. A Lantern Model to Illustrate Dislocations in Crystal Structure 394

Mr. R. Bowers and Dr. K. Mendelssohn. Viscosity and Superfluidity in Liquid Helium 394

Dr. L. E. Beghian and Mr. H. H. Halban. Electron Collection in High Pressure Methane Ionization Chambers 395

Reviews of Books 397

Corrigendum 398

Contents and Abstracts for Section B 399

ABSTRACTS FOR SECTION A

The Structure and Electrical Properties of Surfaces of Semiconductors.—Part I. *Silicon Carbide*, by T. K. Jones, R. A. Scott and R. W. Sillars.

ABSTRACT. Electrical contacts with faces of silicon carbide and of many other semiconductors do not obey Ohm's law. This property of silicon carbide has been attributed to an amorphous film known to occur on faces of the crystal. Theoretical work relating to such contacts is hampered by lack of knowledge of the essential physical features of the model. In this paper a study is made of the manner in which the surface texture of the crystal affects the electrical properties of the contact. The electrical characteristics of a contact between a rounded metal point and the demonstrably smooth face of a crystal were shown to vary only slowly across the surface. A series of observations was made of the electrical properties and of the electron diffraction patterns of a basal plane of a crystal as the overlying film of amorphous material was removed.

The results show that the presence of the amorphous film is not essential to the exhibition of the special electrical properties of the contact.

The Structure and Epitaxy of Lead Chloride Deposits Formed from Lead Sulphide and Sodium Chloride, by A. J. Elleman and H. Wilman.

ABSTRACT. Electron diffraction shows that $PbCl_2$ is formed instead of $PbO . PbSO_2$ when mosaic single-crystal PbS layers a few hundred A. thick are heated on their NaCl substrates in air at 200–300° c. The structure and orientation of these $PbCl_2$ layers are described. This example of epitaxial crystal growth is particularly interesting because the $PbCl_2$ atoms adjacent to the, at least initially, atomically smooth PbS surface do not lie exactly in a single close-packed plane atomic sheet, but the atomic arrangement closely matches that of the PbS substrate in a series of parallel bands. When the composite $PbCl_2$–PbS layers were isolated from their NaCl substrate the transmission patterns showed that they must have partly broken up, leading to curvature about remarkably well-defined axes parallel to the film plane and PbS cube-face diagonals.

On the Absorption Spectrum of Cosmic Rays, by E. W. KELLERMANN and K. WESTERMAN.

ABSTRACT. Attempts at the measurement of the absorption spectrum of cosmic rays by means of counter telescopes have been made by many authors. It is pointed out here that none of the usual methods, i.e. the determination of the number of coincidences as a function of the absorber thickness, can be satisfactory unless the influence of the geometry through scattering is known. Only then can this (integral) absorption curve be used for the determination of the momentum spectrum.

A method of determining directly the differential absorption curve is described which avoids largely the influence of scattering. This method has been used for the investigation of some specific effects which have been observed by some and denied by other authors. In particular, the region of 12 cm. Pb has been investigated, and it is found that the change of absorption observed here is due solely to the overlapping of the high momenta end of the electron spectrum and of the meson spectrum. Although the present investigation cannot confirm it, it does not exclude the possibility of a specific change of the absorption coefficient in the 22 cm. Pb region.

Momentum Spectrum of the Particles in Extensive Air Showers, by S. M. MITRA and W. G. V. ROSSER.

ABSTRACT. An account is given of experiments on the momentum spectrum of the particles in extensive air showers at sea-level. The results are consistent with an integral spectrum of the form $N(>E) \propto (E+E_c)^{-(1{\cdot}1\pm0{\cdot}3)}$, where E_c is the critical energy in air. Penetrating particles are found in some of the denser showers, the ratio of penetrating particles to electrons being $(0{\cdot}8\pm0{\cdot}4)\%$.

The Effect of External Quenching on the Life of Argon–Alcohol Counters, by H. ELLIOT.

ABSTRACT. A simple multivibrator for eliminating multiple discharges in argon–alcohol counters is described. This circuit has been used successfully in cosmic-ray intensity recording equipment requiring a high degree of stability. It is shown that the increase in counter life which is observed when a multivibrator of this kind is used is probably due to quenching of the discharge before it has spread the full length of the counter wire.

On the Absorption of Meson-producing Nucleons, by W. HEITLER and L. JÁNOSSY.

ABSTRACT. The absorption of nucleons passing through any number of nuclei is calculated with due consideration of all fluctuations of energy loss. For the probability $w(\epsilon, E)\,d\epsilon$ for an energy loss ϵ by a nucleon with energy E hitting a nucleon at rest, a law of the form $w\,d\epsilon = w(\epsilon/E)\,d\epsilon/E$ is assumed, a law suggested by meson theory and Bremsstrahlung. It is shown that, with a primary spectrum, following a power law, the absorption is strictly exponential for any thickness of the absorber and for all energies of the nucleons, apart from small deviations at low energies due to the latitude cut-off. This agrees well with recent experimental results. The experiments also permit some conclusions about the shape of the function w, and it is shown that w must be a fairly broad distribution extending up to $\epsilon/E=1$, possibly favouring, but not to a very large extent, low values of ϵ/E. The average energy loss of a fast nucleon hitting a nucleon at rest is determined by the experiments within very narrow limits. The conclusions that can be drawn about w, the total cross-section for meson production and the average energy loss are all compatible with the theory of Hamilton, Heitler and Peng, in its later version.

Some Cut-off Methods for the Electron Self-Energy, by J. RZEWUSKI.

ABSTRACT. Some Lorentz-invariant cut-off procedures for the electron self-energy are investigated. Expressions for the self-energy are obtained as expansions in inverse powers of the cut-off constant K. The first term, logarithmic in K, has the correct transformation properties for all the cut-offs. The second term, independent of K, is covariant only for one of the procedures. The remaining terms have not the correct properties in any of the procedures, but contain negative powers of K and, therefore, vanish for $K \to \infty$. The one cut-off procedure which gives a covariant constant term can, therefore, be used for an unambiguous subtraction of the electron self-energy provided that in the final results one proceeds to the limit $K \to \infty$.